AD-A148 106 NON-LINEAR TRANSVERSE ELECTRON BEAM DYNAMICS IN A MODIFIED BETATRON ACCELERATOR(U) NAVAL RESEARCH LAB WASHINGTON DC C A KAPETANAKOS ET AL. 30 NOV 84 1/1

UNCLASSIFIED NRL-MR-5387 F/G 20/7 NL

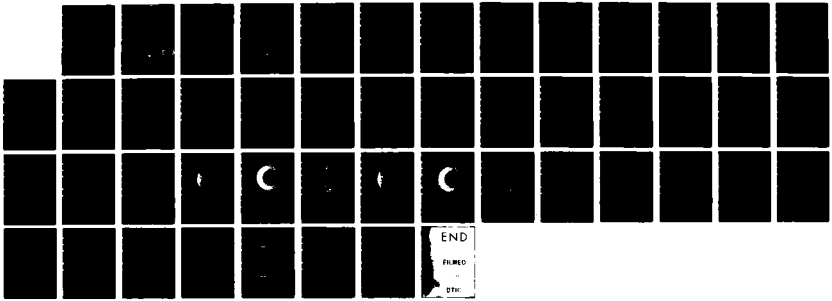

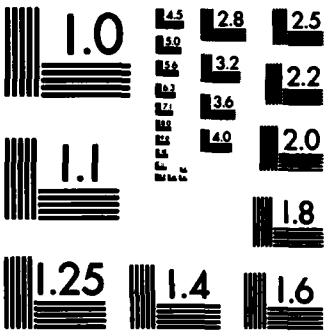

MICROCOPY RESOLUTION TEST CHART
NATIONAL BUREAU OF STANDARDS-1963-A

REPRODUCED AT GOVERNMENT EXPENSE

(2)

NRL Memorandum Report 5387

Non-Linear Transverse Electron Beam Dynamics in a Modified Betatron Accelerator

C. A. KAPETANAKOS AND S. J. MARSH*

Beam Dynamics Program
Plasma Physics Division

**Sachs/Freeman Associates, Inc.*
Bowie, MD 20715

AD-A148 106

November 30, 1984

DTIC
ELECTE
NOV 29 1984
S D
B

DTIC FILE COPY

NAVAL RESEARCH LABORATORY
Washington, D.C.

Approved for public release; distribution unlimited.

84 11 27 043

SECUR CLASSIFICATION OF THIS PAGE

REPORT DOCUMENTATION PAGE

1a. REPORT SECURITY CLASSIFICATION UNCLASSIFIED	1b. RESTRICTIVE MARKINGS
2a. SECURITY CLASSIFICATION AUTHORITY	3. DISTRIBUTION / AVAILABILITY OF REPORT Approved for public release; distribution unlimited.
2b. DECLASSIFICATION / DOWNGRADING SCHEDULE	
4. PERFORMING ORGANIZATION REPORT NUMBER(S) NRL Memorandum Report 5387	5. MONITORING ORGANIZATION REPORT NUMBER(S)
6a. NAME OF PERFORMING ORGANIZATION Naval Research Laboratory 6b. OFFICE SYMBOL (If applicable) Code 4704	7a. NAME OF MONITORING ORGANIZATION Office of Naval Research
6c. ADDRESS (City, State, and ZIP Code) Washington, DC 20375-5000	7b. ADDRESS (City, State, and ZIP Code) Arlington, VA 22217
8a. NAME OF FUNDING / SPONSORING ORGANIZATION 8b. OFFICE SYMBOL (If applicable)	9. PROCUREMENT INSTRUMENT IDENTIFICATION NUMBER
8c. ADDRESS (City, State, and ZIP Code)	10. SOURCE OF FUNDING NUMBERS PROGRAM ELEMENT NO. 61153N; PROJECT NO.; TASK NO. RR011-09-4E; WORK UNIT ACCESSION NO. DN180-280

11. TITLE (Include Security Classification)

Non-Linear Transverse Electron Beam Dynamics in a Modified Betatron Accelerator

12. PERSONAL AUTHOR(S)

Kapetanakos, C.A. and Marsh, S.J.*

13a. TYPE OF REPORT	13b. TIME COVERED	14. DATE OF REPORT (Year, Month, Day)	15. PAGE COUNT
Interim	FROM ____ TO ____	1984 November 30	48

16. SUPPLEMENTARY NOTATION

*Sachs/Freeman Associates, Inc., Bowie, MD 20715

17. COSATI CODES			18. SUBJECT TERMS (Continue on reverse if necessary and identify by block number)
FIELD	GROUP	SUB-GROUP	Accelerators Modified betatron

19. ABSTRACT (Continue on reverse if necessary and identify by block number)

The transverse electron beam dynamics in a modified betatron accelerator is studied using a new approach. This approach is based on the two exact constants of the motion and the potentials at the center of the beam. The main advantage of the present technique is that the ring orbits can be accurately determined over the entire minor cross-section of the torus and not only near the minor axis. Our results indicate that the electron ring orbits, in the plane transverse to the toroidal magnetic field, always close inside the vacuum chamber and their topology is often substantially different than that predicted from the linear theory.

20. DISTRIBUTION / AVAILABILITY OF ABSTRACT ☒ UNCLASSIFIED/UNLIMITED ☐ SAME AS RPT ☐ DTIC USERS	21. ABSTRACT SECURITY CLASSIFICATION UNCLASSIFIED
22a. NAME OF RESPONSIBLE INDIVIDUAL C. A. Kapetanakos	22b. TELEPHONE (Include Area Code) (020) 767-2838 22c. OFFICE SYMBOL Code 4704

DD FORM 1473, 84 MAR 83 APR edition may be used until exhausted. All other editions are obsolete.

SECURITY CLASSIFICATION OF THIS PAGE

CONTENTS

I. INTRODUCTION 1

II. CONSTANTS OF THE MOTION 2

III. THE POTENTIALS 4

IV. TRANSVERSE RING ORBITS 9

V. EXTREME OF THE CONSTANT OF THE MOTION 13

VI. SUMMARY 16

ACKNOWLEDGMENTS 43

REFERENCES 43

DTIC
ELECTE
NOV 29 1984
S D
B

Accession For
NTIS GRA&I ☑
DTIC TAB ☐
Unannounced ☐
Justification
By
Distribution/
Availability Codes
Dist | Avail and/or Special
A-1

NON-LINEAR TRANSVERSE ELECTRON BEAM DYNAMICS IN A MODIFIED BETATRON ACCELERATOR

I. Introduction

High energy accelerators capable of producing high current electron beams are rapidly becoming an active area of research. The motivation for developing these devices is related to potential applications of high current beams to the generation of high power coherent radiation[1], x-ray radiography and national defense[2].

Among the various accelerating schemes that have the potential to produce ultra-high power electron beams, induction accelerators[3] appear to be the most promising. Induction accelerators are inherently low impedance devices and thus are ideally suited to drive high current beams. The acceleration process is based on the inductive electric field produced by a time varying magnetic field. The electric field can be either continuous or localized along the acceleration path.

Quite naturally, induction accelerators are divided into linear and cyclic. The linear devices are in turn divided into Astron-type[4-8], Radlac-type[9,10] and auto-accelerator[11,12]. In the first type, ferromagnetic induction cores are used to generate the accelerating field, while "air core" cavities are used in the second. In the auto-accelerator the air core cavities are excited by the beam's self fields rather than external fields. Similarly, cyclic devices can be divided into conventional[13-15] and modified betatrons[16-20]. The field configuration in the modified betatron includes, in addition to the time varying betatron magnetic field, which is responsible for the acceleration, a strong toroidal magnetic field that substantially improves the stability of the accelerated beam.

The linear dynamics of high current electron rings in modified betatron fields, with and without stellarator fields, has been studied extensively

Manuscript approved July 26, 1984.

during the last few years[16-22]. These studies are based on the linearized equations of motion, i.e., they assume that the electron ring is confined near the minor axis of the torus.

In this paper we study the transverse ring dynamics in a modified betatron accelerator using a different approach. The ring orbits are not determined from the equations of motion but rather from the two exact constants of the motion and the potentials at the centroid of the ring. The main advantage of the present approach is that the ring orbits can be determined over the entire minor cross-section of the torus and not only near its minor axis. The topology of orbits near the wall of the toroidal vacuum chamber is of vital importance during injection, since optimization of the confining region requires the beam to be injected far away from the minor axis of the torus[24,25]. It has been found that the shape of the ring orbits, in the transverse to the toroidal magnetic field plane, can be very complex, in particular in the high current limit.

II. Constants of the Motion

Consider an electron ring inside a perfectly conducting torus of circular cross section as shown in Fig. 1. The center of the ring is located at a distance $\Delta r, \Delta z$ from the minor axis of the torus. The kinetic energy $mc^2\gamma$ of a reference electron that is located at the position r,z varies according to the equation

$$mc^2 \frac{d\gamma}{dt} (r,z) = - |e| \vec{v} \cdot \vec{E} (r,z), \tag{1}$$

where $\vec{E}$ (r,z) is the total electric field at the position of the reference electron. The electric field is related to the space charge ϕ and magnetic

vector potential $\vec{A}$ by

$$\vec{E}\,(r,z) = -\,\nabla\Phi - \frac{1}{c}\,\frac{\partial\vec{A}}{\partial t}\,, \tag{2}$$

where the total time derivative of Φ is given by

$$\frac{d\Phi}{dt} = \frac{\partial\Phi}{\partial t} + \vec{v}\cdot\nabla\Phi. \tag{3}$$

For the problem of interest, the accelerating fields vary slowly in time and thus

$$\frac{\partial\vec{A}}{\partial t} = \frac{\partial\Phi}{\partial t} = 0. \tag{4}$$

Combining Eqs. (1) to (4), we obtain

$$\frac{d\gamma(r,z)}{dt} - \frac{|e|}{mc^2}\,\frac{d\Phi(r,z)}{dt} = 0$$

or

$$\gamma(r,z) - \frac{|e|}{mc^2}\,\Phi(r,z) = \text{constant}. \tag{5}$$

According to Eq. (5) the sum of the kinetic and potential energy of the reference electron is conserved.

Since the fields of the modified betatron configuration are independent of the toroidal angle θ, the canonical angular momentum P_θ is also a constant of the motion, i.e.,

$$P_\theta = \gamma\, mr\, v_\theta - \frac{|e|}{c}\, r\, A_\theta = \text{constant}, \tag{6}$$

where A_θ is the toroidal component of the total magnetic vector potential and v_θ is the toroidal velocity of the reference electron.

Assuming that $v_\theta \approx v$ and eliminating γ from Eqs. (5) and (6), it is obtained

$$\left[\left(\frac{P_\theta}{mcr} + \frac{|e|}{mc^2} A_\theta(r,z)\right)^2 + 1\right]^{1/2} - \frac{|e|}{mc^2}\Phi(r,z) = \text{constant}, \tag{7a}$$

or, at the centroid of the ring

$$\left[\left(\frac{P_\theta}{mcR} + \frac{|e|}{mc^2} A_\theta(R,Z)\right)^2 + 1\right]^{1/2} - \frac{|e|}{mc^2}\Phi(R,Z) = \text{constant}. \tag{7b}$$

For very high energy beams, i.e., when $\gamma^2 \gg 1$, Eq. (7b) is reduced to

$$\frac{P_\theta}{mcR} + \frac{|e|}{mc^2}\left[A_\theta(R,Z) - \Phi(R,Z)\right] = \text{constant}. \tag{7c}$$

This non-linear conservation law can furnish very useful information on the motion of the ring in the r,z plane, provided that the potentials A_θ and Φ at the center of the ring are known. It should be noticed that Eqs. (7) are independent of the toroidal magnetic field.

III. The Potentials

In Eq. (7), the total magnetic vector potential $A_\theta(r,z)$ is

$$A_\theta(r,z) = A_\theta^{ext}(r,z) + A_\theta^{self}(r,z),$$

where $A_\theta^{ext}(r,z)$ is the external and $A_\theta^{self}(r,z)$ is the self magnetic vector potential.

It is assumed that the betatron magnetic field is described by

$$A_\theta^{ext}(r,z) = B_{zo}\left[\left(\frac{r_o}{r}\right)^n \left(\frac{r}{2-n}\right) + \frac{r_o^2}{r}\frac{(1-n)}{(2-n)} + \frac{nz^2}{2r}\right], \tag{8}$$

where B_{zo} is the magnetic field at $r=r_o$, $z = o$ and n is the external field index, i.e.,

$$n = -\frac{r_o}{B_{zo}}\left(\frac{\partial B_z}{\partial r}\right)_{r_o,o} .$$

For a cylindrical electron beam inside a straight perfectly conducting cylindrical pipe of circular cross section, the self potentials can be computed exactly, even for large beam displacements from the minor axis of the torus. In the local coordinate system ρ,ϕ the self potentials inside the beam, i.e., for $|\vec{\rho}-\vec{\Delta}| < r_b$ are given by

$$A_\theta^{self}(\rho,\phi) = -2|e|\, N_\ell\, \beta_\theta \left\{ \tfrac{1}{2} + \ln\frac{a}{r_b} - \frac{[\rho^2+\Delta^2-2\rho\,\Delta\cos(\phi-\alpha)]}{2r_b^2} \right.$$

$$\left. - \sum_{\ell=1}^{\infty}\left(\frac{\rho}{a}\right)^\ell\left(\frac{\Delta}{a}\right)^\ell \ell^{-1}\cos(\phi-a)\right\}, \tag{9a}$$

and

$$\Phi(\rho,\phi) = -2|e|\, N_\ell \left\{ \tfrac{1}{2} + \ln\frac{a}{r_b} - \frac{[\rho^2+\Delta^2-2\rho\,\Delta\cos(\phi-\alpha)]}{2\,r_b^2} \right.$$

$$\left. - \sum_{\ell=1}^{\infty}\left(\frac{\rho}{a}\right)^\ell\left(\frac{\Delta}{a}\right)^\ell \ell^{-1}\cos(\phi-\alpha)\right\}, \tag{9b}$$

At the beam center, i.e., for $\rho = \Delta$ and $\phi = \alpha$, Eqs. (9a) and (9b) become

$$A_\theta^{self}(R,Z) = -2\,|e|N_\ell\,\beta_\theta\,\{\tfrac{1}{2} + \ln\frac{a}{r_b} + \ln\,[1 - \frac{(R-r_o)^2 + Z^2}{a^2}]\}, \quad (10a)$$

and

$$\Phi(R,Z) = -\,2\,|e|\,N_\ell\,\{\tfrac{1}{2} + \ln\frac{a}{r_b} + \ln\,[1 - \frac{(R-r_o)^2 + Z^2}{a^2}]\}, \quad (10b)$$

where N_ℓ is the linear electron density, r_b is the minor radius of the beam, a is the minor radius of the conducting pipe and $\beta_\theta = v_{\theta/c}$.

Figure 2 shows the ratio $-A_\theta^{self}/2N_\ell\,|e|\,(v_{\theta/c})$ from Eq. (10a) at Z = o, together with results from the computer code PANDIRA. This code solves the differential equations for $\vec{A}$ and Φ in a non-uniform triangular mesh in r-z coordinates and its present version has been developed by R.F. Holsinger. The various parameters for the runs shown in Figs. 2 to 5 are listed in Table I. The agreement between Eq. (10a) and the numerical results is excellent. The maximum difference between the analytical and numerical results is less than 0.4%.

Figure 3 shows the stream function $\psi = RA_\theta^{self}$. In contrast to A_θ^{self}, the stream function ψ peaks away from the minor axis of the torus. The radial displacement of the peak can be computed from $\partial\psi/\partial R = 0$ and is given by the relation

$$\Delta_\rho \approx (a/2)\,(a/r_o)\,(\tfrac{1}{2} + \ln a/r_b).$$

This relation predicts that ψ peaks 2.8 cm from the minor axis, which is not by far-off from the 2.6 cm of Fig. 3.

Results for the electrostatic potential are given in Fig. 4. Again the agreement between Eq. (10b) and numerical results is excellent. The maximum

difference $\Delta\Phi$ between the electrostatic potential computed from PANDIRA and that of Eq. (10b) is less than 2%.

Figure 5 shows the stream function ψ for a torus with a major radius r_o = 32 cm. In agreement with the approximate expression for Δ_ρ, the displacement of the peak increased by about a factor of 3.

To obtain a better understanding of the potentials inside a perfectly conducting torus, we solved[26] the differential equations for Φ and $\vec{A}$ to first order in the ratio a/R, but to any order in the normalized displacement Δ/a.

For a constant particle density n_o ring and to second order in Δ/a, the electrostatic potential and the stream function ψ at the center of the ring are given by

$$\Phi(R,Z) = -2\,N_\ell\,|e|\,\left[\tfrac{1}{2} + \ln(a/r_b) - \frac{(R-r_o)^2 + Z^2}{a^2} - \frac{r_b^{\,2}}{8a^2}\left(\frac{R-r_o}{R}\right)\right], \tag{11a}$$

$$\psi(R,Z) = -2\,N_\ell\,|e|\,R\,\beta_\theta\left[\tfrac{1}{2} + \ln(a/r_b) - \frac{(R-r_o)^2 + Z^2}{a^2} - \frac{3r_b^{\,2}}{8a^2}\left(\frac{R-r_o}{R}\right)\right], \text{ for } \dot{\theta} = \text{constant} \tag{11b}$$

and

$$\psi(R,Z) = -2N_\ell|e|R\beta_\theta\left[1/2 + \ln(a/r_b) - \frac{(R-r_o)^2 + Z^2}{a^2} - \frac{r_b^{\,2}}{8a^2}\frac{(R-r_o)}{R}\right],$$

$$\text{for } J_\theta = \text{constant}. \tag{11c}$$

Similarly, the fields at the centroid of the ring are given by

$$E_r = -\frac{2|e|N_\ell}{a}\left[\frac{(R-r_o)}{a} + \left(\frac{a}{2R}\right)\ \ell n\ \frac{a}{r_b} + \frac{r_b^{\ 2}}{8Ra}\right], \tag{12a}$$

$$E_z = -\frac{2|e|N_\ell}{a}\left(\frac{Z}{a}\right), \tag{12b}$$

$$B_r = -\frac{2|e|N_\ell\beta_\theta}{a}\left(\frac{Z}{a}\right), \tag{12c}$$

$$B_z = \frac{2|e|N_\ell\beta_\theta}{a}\left[\frac{(R-r_o)}{a} - \left(\frac{a}{2R}\right)\left(\ln\ \frac{a}{r_b} + 2\right)\right.$$

$$\left. + (3r_b^{\ 2}/8Ra)\right], \text{ for } \dot{\theta} = \text{constant}, \tag{12d}$$

and

$$B_z = \frac{2|e|N_\ell\beta_\theta}{a}\left[\frac{(R-r_o)}{a} - \left(\frac{a}{2R}\right)\left(\ell n\ \frac{a}{r_b} + 1\right)\right.$$

$$\left. + \left(\frac{r_b^{\ 2}}{8Ra}\right)\right], \text{ for } J_\theta = \text{constant}. \tag{12e}$$

The toroidal term in Eq. (11) is very small for the parameters of interest and therefore it is not surprising that the potential at the center of the ring are approximately cylindrical.

For low energy rings the small toroidal term could be important and could have a profound effect on the shape of the orbits. However, when $\gamma \gg 1$, the potentials for n_o = constant and J_θ = constant become approximately equal and hence they do not contribute substantially in Eq. (7c).

IV. Transverse Ring Orbits

Equation (7b) has been solved numerically, using the potentials of Eq. (11). Typical macroscopic beam orbits in the r,z plane are shown in Figs. 6 to 8. The various parameters for those runs are listed in Table II. Only orbits that are at least one beam minor radius away from the wall are shown. Each orbit corresponds to a different value of the constant in Eq. (7b). A striking feature of the results is the sensitivity of the orbits to the value of the constant in Eqs. (7).

The number marked in every fourth orbit is equal to 10^4 [constant - <constant>], where the average value of the constant, i.e. <constant> for each run is shown at the top of the figure. For all the cases tested, less than 3% change in the constant of the motion was sufficient to generate orbits that extend over the entire minor cross-section of the torus. Orbits shown with solid lines correspond to a constant that is greater than <constant> and those shown with a dashed line correspond to a constant that is less than <constant>.

All the orbits close inside the vacuum chamber. However, a fraction of them lie inside the annular region that extends from the dotted-dashed line to the wall. This region has a width that is less than the beam radius and hence part of the beam will strike the wall.

Ring orbits in the r,z plane from Eq. (7b) using the potentials of Eq. (10), i.e., emitting the toroidal terms, are shown in Figs. 9 to 11. It is apparent that there is not any noticeable difference between these orbits and those of Figs. 6 to 8.

The predictions of Eq. (7b) are in very good agreement with the results from our particle in cell (PIC) computer simulation.[20] Figures 12 to 14 show three computer simulation runs. As may be seen from Table III, with the exception of the betatron field, the various parameters in the simulation are the same with those of Figs. 6 to 8. The slightly lower value of the betatron field in Figs. 12 to 14 is related to the different radial profiles for J_θ in the simulation and the potentials of Eq. (11). The orbit wiggles are due to the finite ring emittance, which was taken zero in the derivation of Eq. (7b). It should be noticed that in these computer simulation runs the electron ring was reasonably well matched to the magnetic field as it is manifested from the small variations in the axial and radial ring envelopes shown in Fig. 15.

In the general case, it is difficult to derive an explicit expression for the ring orbits in the transverse plane from Eqs. (7b) and (11). However, in the limit $\gamma^2 \gg 1$, $\beta_\theta/\beta \simeq 1$ and $\nu/\gamma \ll 1$, such an expression can be obtained near the minor axis of the torus.

Since $\beta_\theta \simeq \beta$ and $\gamma\beta \simeq \gamma - 1/2\gamma$, Eqs. (5)and (6) give

$$\frac{P_\theta}{mcR} + \frac{|e|}{mc^2} A_\theta^{ext} + \frac{|e|}{mc^2} \left(A_\theta^{self} - \Phi\right) + \frac{1}{2\gamma} = \text{constant} = G. \qquad (13)$$

Expanding γ near r_o and using Eq. (5), it is obtained

$$\delta\gamma = \gamma - \gamma_o = \frac{|e|}{mc^2} \frac{\partial\Phi}{\partial r}\Big|_{r_o} \Delta r + \frac{\partial G}{\partial r}\Big|_{r_o} \Delta r,$$

where $\Delta r = R - r_o$. It is shown in the next section that $\frac{\partial G}{\partial r}\Big|_{r_o} = 0$ and thus the above equation becomes

$$\delta\gamma = \gamma - \gamma_o = \frac{|e|}{mc^2} \frac{\partial\Phi}{\partial r}\Big|_{r_o} \Delta r. \qquad (14)$$

From Eqs. (11a) and (11c), the difference in the self potentials can be written as

$$A_\theta^{self} - \Phi = 2N_\ell \, |e| \, \{1/2 + \ell n \frac{a}{r_b} - \frac{\Delta r^2 + \Delta Z^2}{a^2} - \frac{r_b^{\,2}}{8a^2} \frac{\Delta r}{R} \} \, (1-\beta_\theta). \qquad (15)$$

Since

$1-\beta_\theta \simeq 1-\beta \simeq 1/2\gamma^2$ and substituting $\delta\gamma$ from Eq. (14) in the expansion for $1/\gamma^2$, it is obtained

$$1-\beta_\theta \simeq \frac{1}{2\gamma_o^2} \left[1 - \frac{2}{\gamma_o} \frac{|e|}{mc^2} \left.\frac{\partial\Phi}{\partial r}\right|_{r_o} \Delta r\right]. \qquad (16)$$

Similarly, expanding $1/2\gamma$ as

$$\frac{1}{2\gamma} \simeq \frac{1}{2\gamma_o} - \frac{|e|}{2\gamma_o^2 mc^2} \left.\frac{\partial\Phi}{\partial r}\right|_{r_o} \Delta r, \qquad (17)$$

and $1/R$ as

$$\frac{1}{R} \simeq \left(\frac{1}{r_o}\right) \left[1 - \frac{\Delta r}{r_o} + \left(\frac{\Delta r}{r_o}\right)^2 \right], \qquad (18)$$

and using a linear expression for the external vector potential

$$A_\theta^{ext} \simeq B_{zo} r_o \left[1 + \frac{\Delta r^2 (1-n)}{2r_o^{\,2}} + \frac{\Delta Z^2 n}{2r_o^{\,2}} \right], \qquad (19)$$

Eqs. (13) to (19) give

$$\left[\frac{P_\theta}{mcr_o} + \frac{\Omega_{zo}^{ext}\, r_o}{2c}(1-n) - \frac{\nu r_o^2}{\gamma_o^2 a^2}\right]\left(\frac{\Delta r}{r_o}\right)^2 + \left[\frac{\Omega_{zo}^{ext} r_o}{2c} n - \frac{\nu r_o^2}{\gamma_o^2 a^2}\right]\left(\frac{\Delta z}{r_o}\right)^2$$

$$- \left[\frac{P_\theta}{mcr_o} + \frac{\nu}{2\gamma_o^2}\left(\frac{r_b^2}{2a^2} + \ln\frac{a}{r_b}\right)\right]\left(\frac{\Delta r}{r_o}\right) = \tilde{G}\ , \qquad (20)$$

where

$$\Delta r = R - r_o,\ \Delta z = Z,\ \tilde{G} = G - \left[\ 1/2\gamma_o^2 + P_\theta/mcr_o\right.$$

$$\left. + \left(\nu/\gamma_o^2\right)\left(1/2 + \ln\frac{a}{r_b}\right) + \Omega_{zo}^{ext}\ r_o/c\right],\ \Omega_{zo}^{ext} = |e|\ B_{zo}^{ext}/mc,$$

and ν is the Budker's parameter.

Equation (20) describes the ring orbits near the minor axis, when $\gamma^2 \gg 1$. These orbits are centered around the minor axis of the torus when the coefficient of the $\left(\frac{\Delta r}{r_o}\right)$ term is zero, i.e., when

$$\frac{P_{\theta o}}{mcr_o} = -\frac{\nu}{2\gamma_o^2}\left[\left(\frac{r_b}{2a}\right)^2 + \ln\frac{a}{r_b}\right] \qquad (21)$$

For $(r_b/a)^2 \ll 1$ and $\gamma_o \gg 1$, Eq. (21) predicts that $\frac{P_\theta}{mcr_o} \approx 0$. Therefore, the orbits are circular when the external field index is approximately equal to 0.5, in agreement with the computer results shown in Figs. 7 and 13.

This result is not in agreement with previous work,[19,20,22] which for J_θ = constant predicts circular orbits when

$$n \approx \frac{1}{2}\,\frac{\left[\ 1 - (\nu/\gamma_o)\ \ln\left(\frac{a}{r_b}\right)\ \right]}{1 + \left(2\nu/\gamma_o\right)\left[1/2 + \ln\frac{a}{r_b}\right]}\ . \qquad (22)$$

It has been determined that the discrepancy is due to an inconsistency in the expansion that gave erroneous results for the two slow frequencies ω_r and ω_z and made the expression for the field index, i.e., Eq. (22), invalid.

Additional results from Eq. (7b) are shown in Figs. (16) to (19). The various parameters for these runs are listed in Table IV. As the ring current increases, the orbits are dramatically modified as manifested by the results of Fig. 18. Midway to the wall, the orbits change from circles to finite width C shaped forms that evolve to cresents or "bananas". At the tips of the crescents the bounce frequency becomes zero and the macroscopic beam motion transitions from diamagnetic to paramagnetic and vice versa. Particle in cell computer simulation results show that the beam can go through such a transition without any noticeable interruption. A typical case is shown in Fig. 20. The various parameters of this run, that lasted for more than 1 microsecond, are listed in Table V. Figure 20a shows the orbit of the center of the ring in the r,z plane. The time interval beween two successive dots is 20 nsec. According to Figs. 20b and 20c the ring envelope changes only slightly during the run.

V. Extreme of the Constant of the Motion

The extreme of Eq. (5) furnishes useful information on the dynamics of the ring in the r-z plane. First, we will show that this extreme is the radial balance equation of motion for the reference electron.

Setting the partial derivative of Eq. (5) with respect to r equal to zero

$$\frac{\partial \gamma}{\partial r} - \frac{|e|}{mc^2} \frac{\partial \Phi}{\partial r} = 0, \tag{23}$$

and using the relation $\gamma = (1 + \beta^2\gamma^2)^{1/2}$ and Eq. (6), we obtain

$$\frac{\partial\gamma}{\partial r} = \beta \left[- \frac{P_\theta}{mcr^2} + \frac{|e|}{mc^2} \frac{\partial A_\theta^{ext}}{\partial r} + \frac{|e|}{mc^2} \frac{\partial A_\theta^{self}}{\partial r} \right], \tag{24}$$

where we have assumed that $\beta = v/c$ is approximately equal to $\beta_\theta = v_\theta/c$. Substituting Eq. (6) into Eq. (24) and using the equations

$$B_z^{ext} = \frac{A_\theta^{ext}}{r} + \frac{\partial A_\theta^{ext}}{\partial r}, \tag{25a}$$

$$B_z^{self} = \frac{A_\theta^{self}}{r} + \frac{\partial A_\theta^{self}}{\partial r}, \tag{25b}$$

and

$$E_r = - \frac{\partial\phi}{\partial r}, \tag{25c}$$

it is obtained

$$- \gamma m \frac{v_\theta^2}{r} = - |e| \left[E_r + \frac{v_\theta}{c} (B_z^{ext} + B_z^{self})\right], \tag{26}$$

i.e., the radial balance equation. This equation gives the equilibrium position of the ring, which is located along the $\hat{e}_r$ axis. At this position the reference electron at the centroid of the ring moves only along the toroidal direction, i.e, $v_r = v_z = 0$.

When the equilibrium position is at $r = r_o$, the toroidal velocity of the reference electron can be determined from Eqs. (6) and (21) and is

$$v_{\theta o} = \frac{r_o \Omega^{ext}_{zo} / \gamma_o - \frac{\nu}{2\gamma_o^3} \left[\left(\frac{r_b}{2a}\right)^2 + \ln \frac{a}{r_b} \right]}{\left[1 + \frac{2\nu}{\gamma_o} \left(1/2 + \ln \frac{a}{r_b} \right) \right]} . \tag{27}$$

With the exception of the very small term on the numerator, Eq. (27) is the same with the expression reported previously (20) for beams with square current density profile.

The external magnetic field B^{ext}_{zo} required to confine the ring at $r = r_o$ can be readily found from Eq. (27). Omitting the small term in the numerator of Eq. (27), we obtain

$$B^{ext}_{zo} = B^{sp}_{zo} \left[1 + \frac{2\nu}{\gamma_o} \left(1/2 + \ln \frac{a}{r_b}\right)\right], \tag{28}$$

where the single particle magnetic field is $B^{sp}_{zo} = \frac{\gamma_o \beta_o}{r_o} \frac{mc^2}{|e|}$.

The magnetic field required to maintain the beam at an equilibrium position that is different than r_o can also be determined from the radial balance equation. Substituting E_r and B^{self}_z from Eqs. (12a) and (12e) into Eq. (26), it is obtained

$$B^{ext}_z = B^{sp}_z \left\{ 1 + \frac{2\nu}{\gamma} \left[1/2 + \ln \frac{a}{r_b} + \frac{R(R-r_o)}{a^2 (\gamma\beta)^2} + \frac{r_b^2}{8a^2 (\gamma\beta)^2} \right] \right\} \tag{29}$$

Equation (29) has been derived under the assumption that ν is not a function of R.

The predictions of Eq. (29) are in excellent agreement with the result of the NRL computer simulation code. Three examples are shown in Table VI.

VI. Summary

The non-linear beam dynamics in the plane transverse to the toroidal magnetic field is studied using the two constants of the motion, instead of the linearized equations of motion. This approach allows the beam orbits to be determined over the entire minor cross-section of the torus and not only near the minor axis.

It was found that the orbits are sensitive to the external field index, to the value of the constant of Eqs. (7) and to the beam current. The orbits in the r,z plane always close inside the vacuum chamber, although often very near the perfectly conducting wall. As a result, beam interruption will occur whenever the electron ring moves along one of these orbits.

In addition, it has been shown that the extreme of Eq. (5) provides information on the external magnetic field required to confine the ring at its equilibrium position and the displacement of the equilibrium position when the beam energy is not matched to the vertical field.

Table I

Parameters for the runs shown in Figs. (2) to (5)

Parameter	Fig. 2	Fig. 3	Fig. 4	Fig. 5
Torus major radius r_o (cm)	100	100	32	32
Torus minor radius a (cm)	16	16	16	16
Electron ring minor radius r_b (cm)	3	3	3	3
Electron ring vertical displacement Z (cm)	0	0	0	0

Table II

Parameters for the results shown in Figs. (6) to (8)

	Fig. 6	Fig. 7	Fig. 8
External field index	0.35	0.5	0.65
Torus major radius (m)	100	100	100
Torus minor radius (cm)	16	16	16
Ring minor radius (cm)	3	3	3
Ring current (kA)	5	5	5
Electron energy (MeV)	3.123	3.123	3.123
Betatron field B_{zo} (G)	138.4	138.5	138.5
P_θ/mcr_o	-0.0018	-0.0020	-0.0023

Table III

Parameters of the computer simulation runs in Figs. (12) to (14)

	Fig. 12	Fig. 13	Fig. 14
External field index n	0.35	0.5	0.65
Initial beam energy γ_o = 7.117			
Beam current I (kA) = 5 KA			
Torus major radius r_o (cm) = 100			
Initial beam minor radius r_b (cm) = 3			
Torus minor radius a (cm) = 16			
Betatron magn. field at r_o, z = o, B_{oz} (G) = 136.2			
Toroidal magn. field at r_o, z = o, $B_{o\theta}$ (G) = 388			
Initial emittance ϵ (rad - cm) = 0.1			

Table IV

Parameters for the runs shown in Figs. (16) to (19)

Cylindrical Potentials

Parameter	Fig. 16	Fig. 17	Fig. 18	Fig. 19
Torus major radius r_o (cm)	100	100	100	100
Torus minor radius a (cm)	16	16	16	16
Electron ring minor radius r_b (cm)	3	3	3	3
Electron ring energy E (MeV)	1.0	1.0	3.0	1.0
Electron ring current I (kA)	1.0	2.0	10.0	1.0
External field index η	0.5	0.5	0.5	0.5
Equilibrium position R_{eq}	100	100	100	112
Vertical magnetic field B_{zo} (G)	51.74	56.08	159.24	53.52
Norm. canonical angular momentum P_{θ}/mcr_o	0	0	0	-2.37×10^{-3}

Table V

Parameters of the computer simulation run shown in Fig. 20.

Run No. D1/111.50

Initial beam energy $\gamma_o = 2.76$ (E = 0.9 MeV)
Beam Current I (kA) = 1
Major radius r_o (cm) = 100
Initial beam minor radius r_b (cm) = 2.5
Torus minor radius a (cm) = 16
Initial beam center position r_i (cm) = 111.0
Betatron magn. field at r_o, z = o, B_{oz} (G) = 47
Toroidal magn. field at r_o, z = o, $B_{o\theta\ (KG)} = 400$
Initial emittance ϵ (rad - cm) = 0.175
Initial temperature spread (half-width) $\frac{\Delta\gamma}{\gamma} = 0$
External field index n = 0.5
Self field index $n_s = 8.6$
Wall conductivity = ∞
Time step (nsec) = 0.10
No. of particles = 2048

Table VI

External magnetic field B_z^{ext} required to maintain the electron ring at its equilibrium position $R \neq r_o$

Energy (γ)	Current (kA)	Torus major radius (cm)	Equilibrium Position (cm)	Torus minor radius (cm)	Ring minor radius (cm)	B_z^{ext}(G) Simulation	B_z^{ext}(G) From Eq. 29
6.34	10	100	104.5	6.4	1.0	150.0	149.9
2.76	1	100	111	16	2.5	44.6	44.7
2.68	1	100	113	16	2.5	43.7	44.1

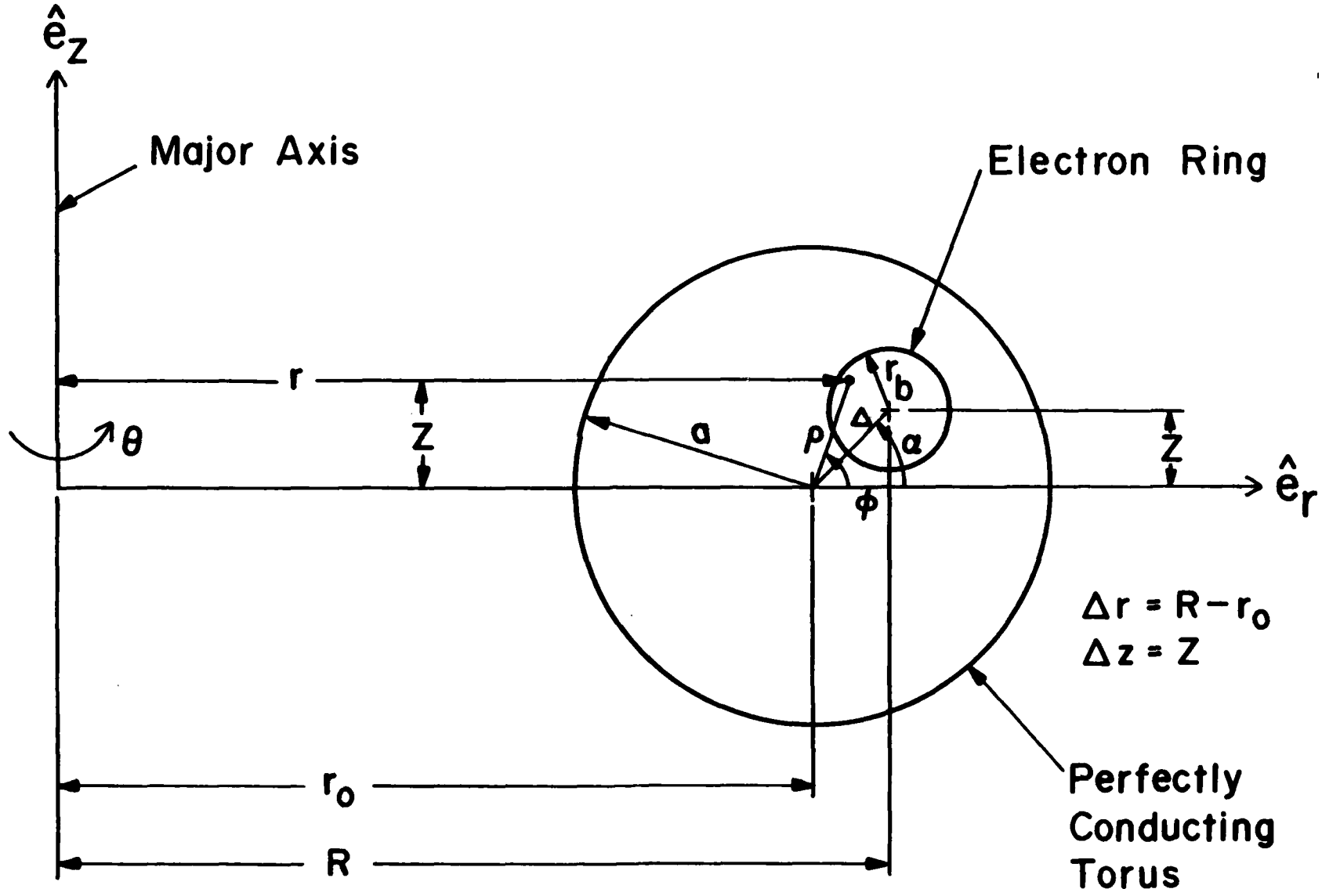

Fig. 1. System of coordinates.

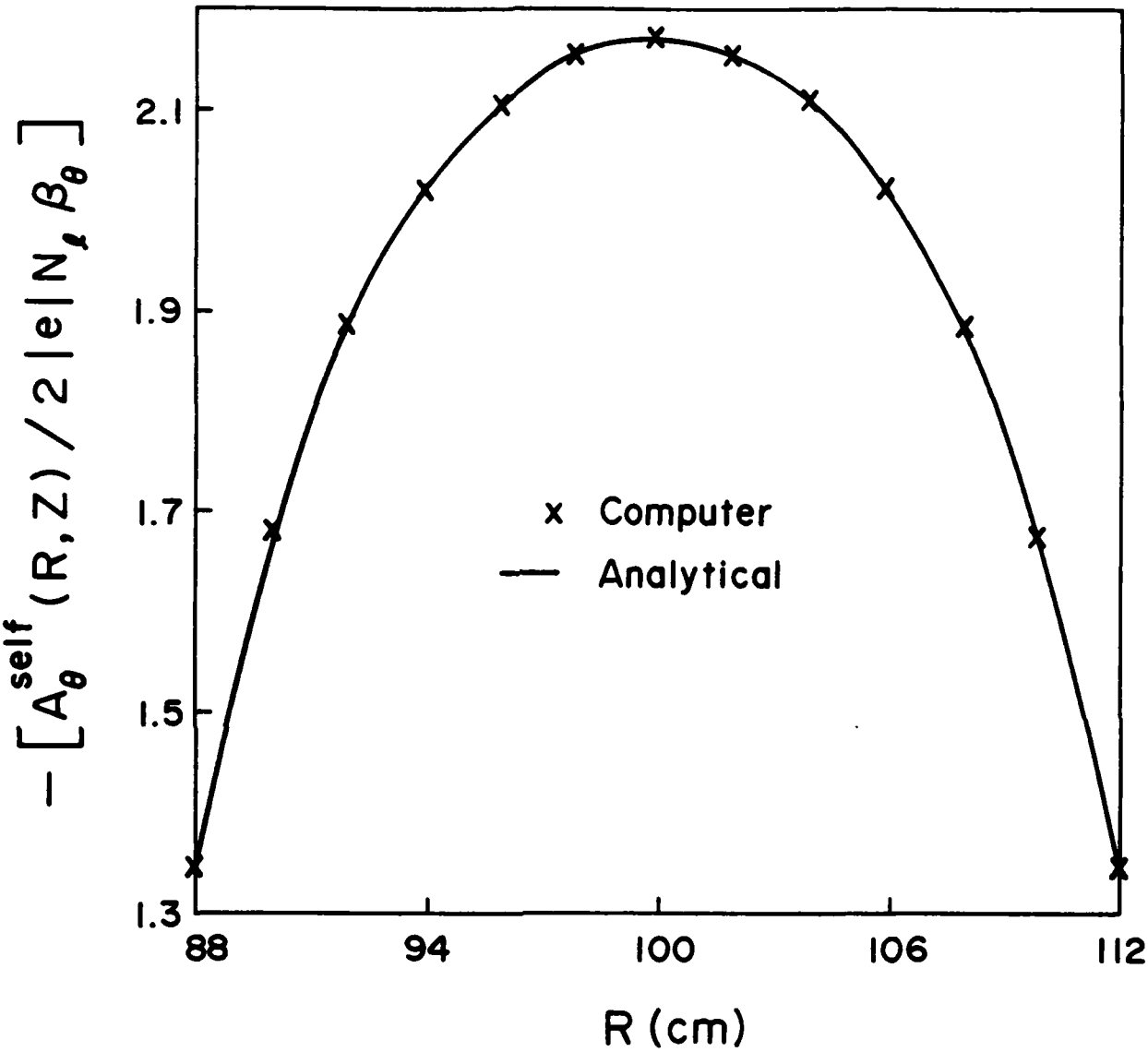

Fig. 2. Normalized self magnetic vector potential from Eq. (10a) and from computer code PANDIRA. The various parameters are listed in Table I.

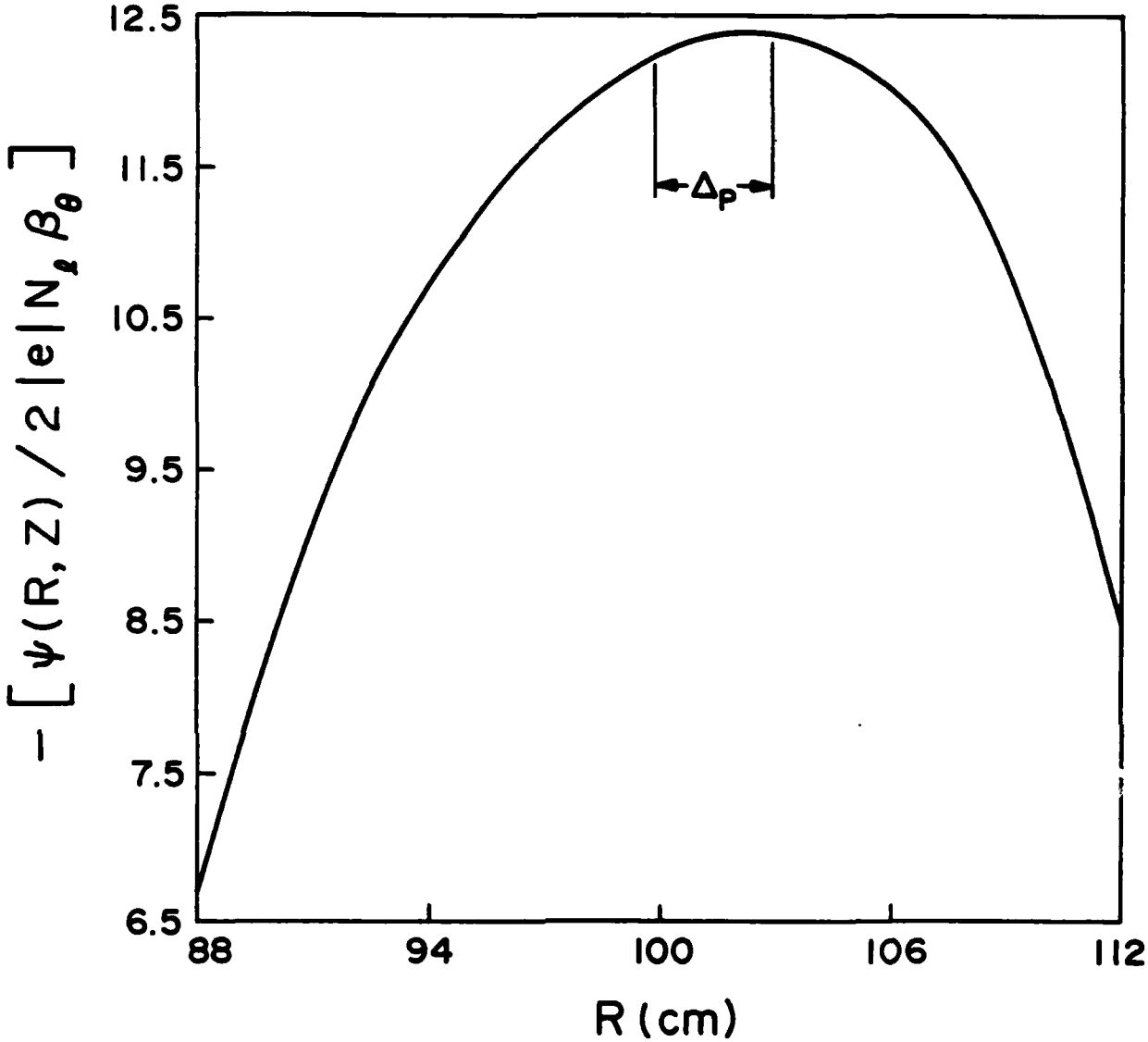

Fig. 3. Normalized self stream function $\psi = RA_\theta^{self}$ as a function of radial distance R. The various parameters are listed in Table I.

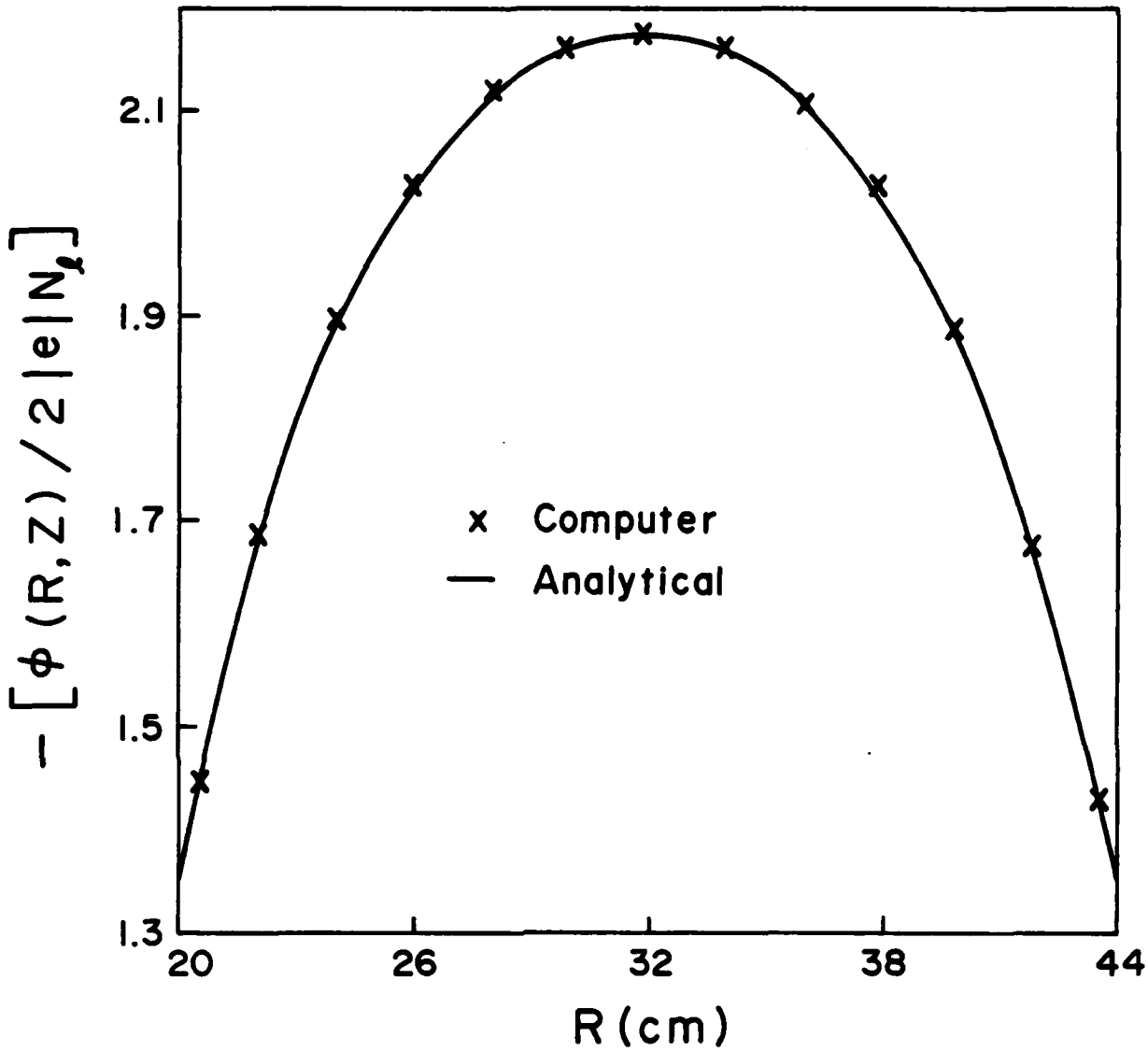

Fig. 4. Normalized self electric potential as a function of R from Eq. (10b) and computer code PANDIRA. The various parameters are listed in Table I.

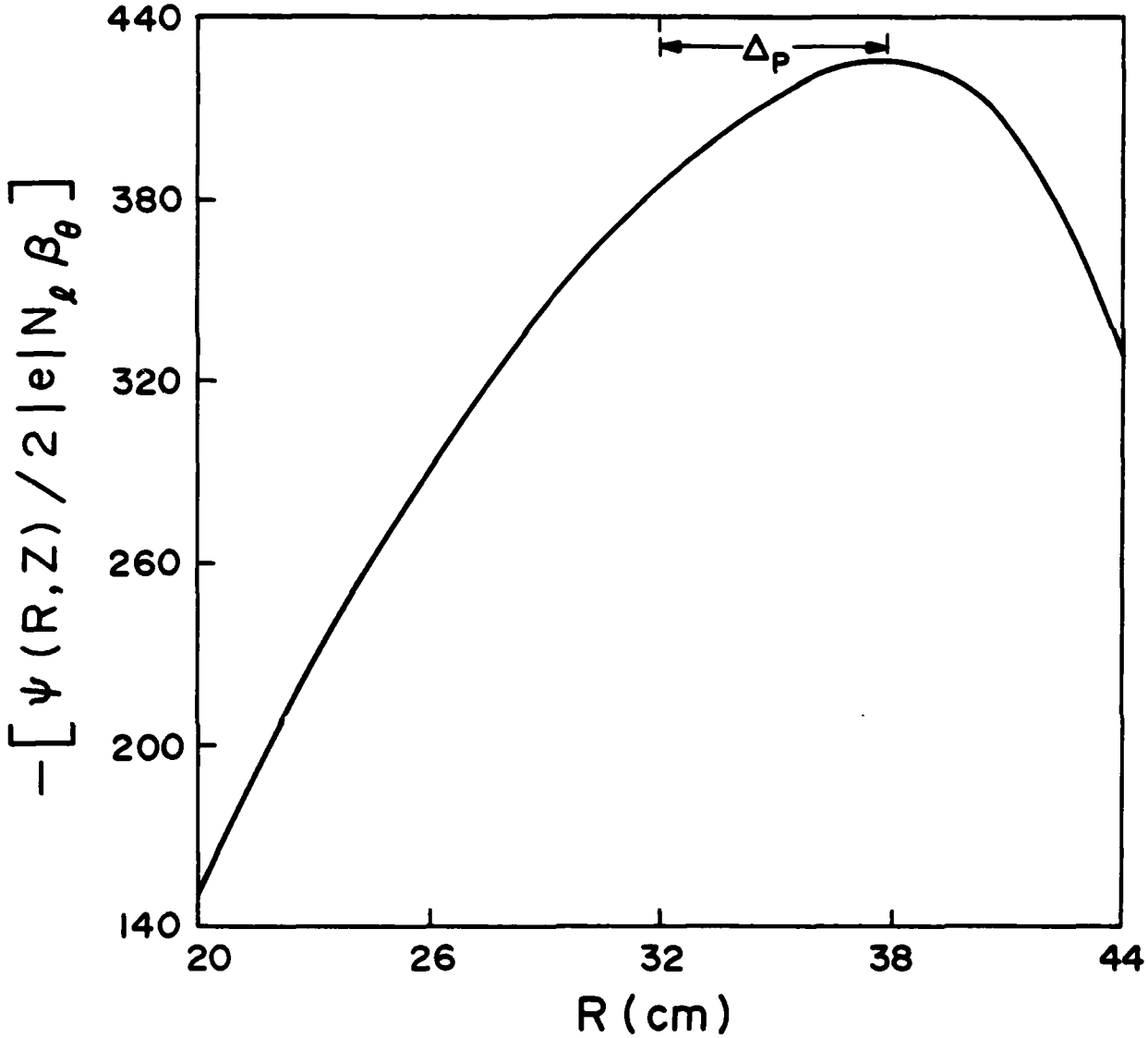

Fig. 5. Normalized self stream function $\psi = RA_\theta^{self}$ as a function of radial distance R for a smaller major radius torus than Fig. 3. The various parameters are listed in Table I.

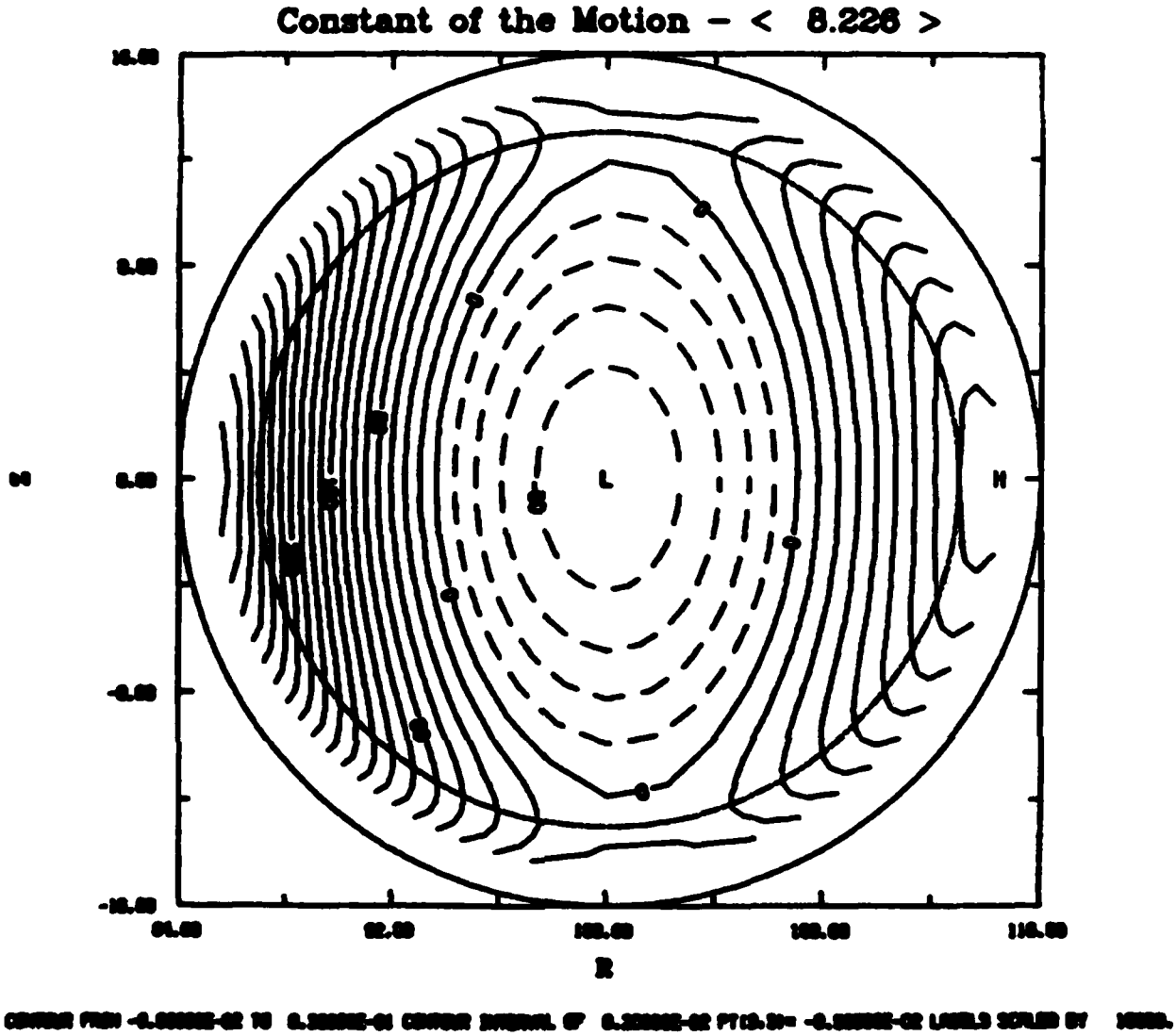

Fig. 6. Orbits of the ring centroid in the transverse plane from Eq. (7b) and the potential of Eq. (11), for an external field index n = 0.35. The rest of the parameters are listed in Table II.

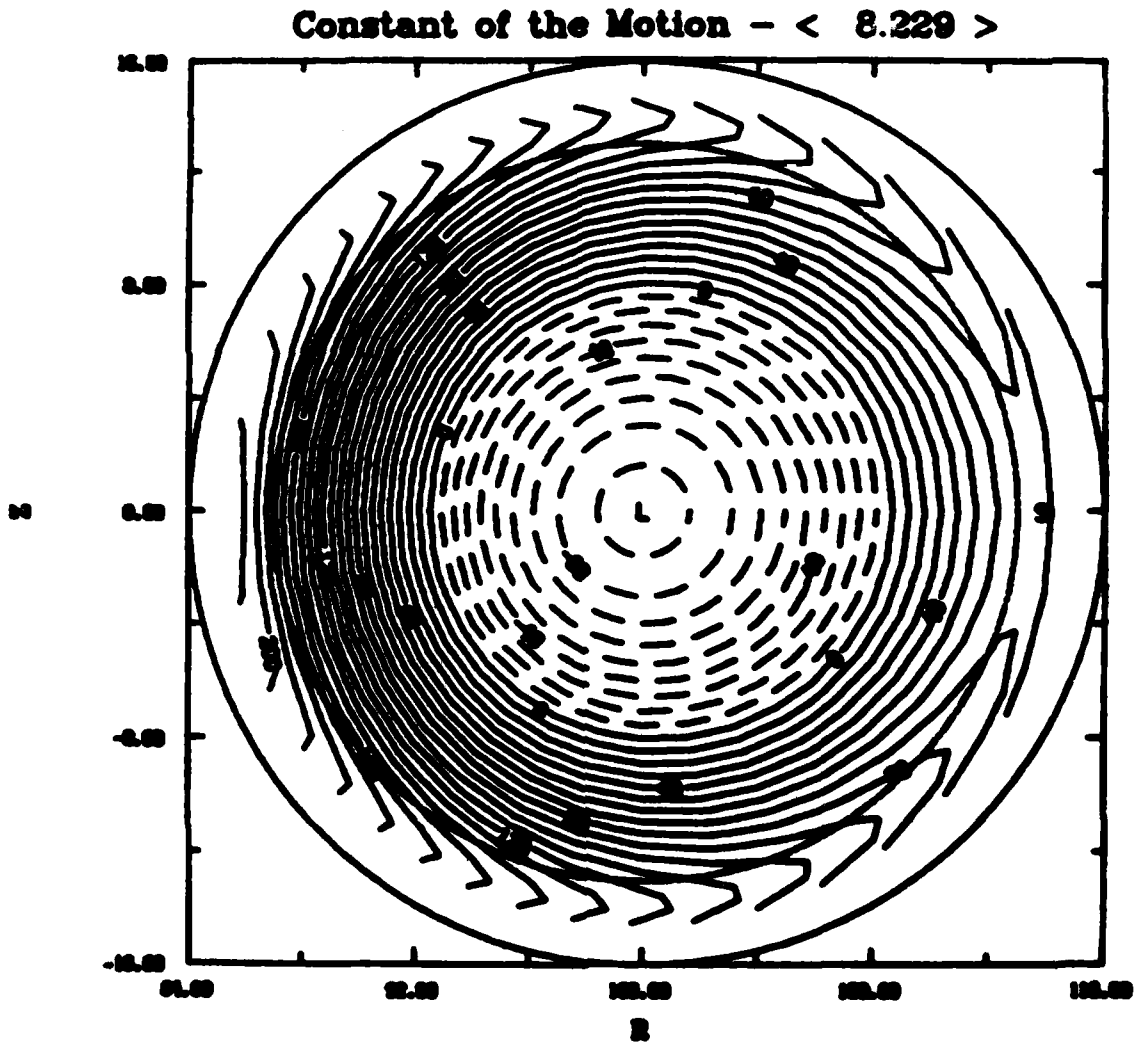

Fig. 7. Orbits of the ring centroid as in Fig. 6, but with n = 0.5.

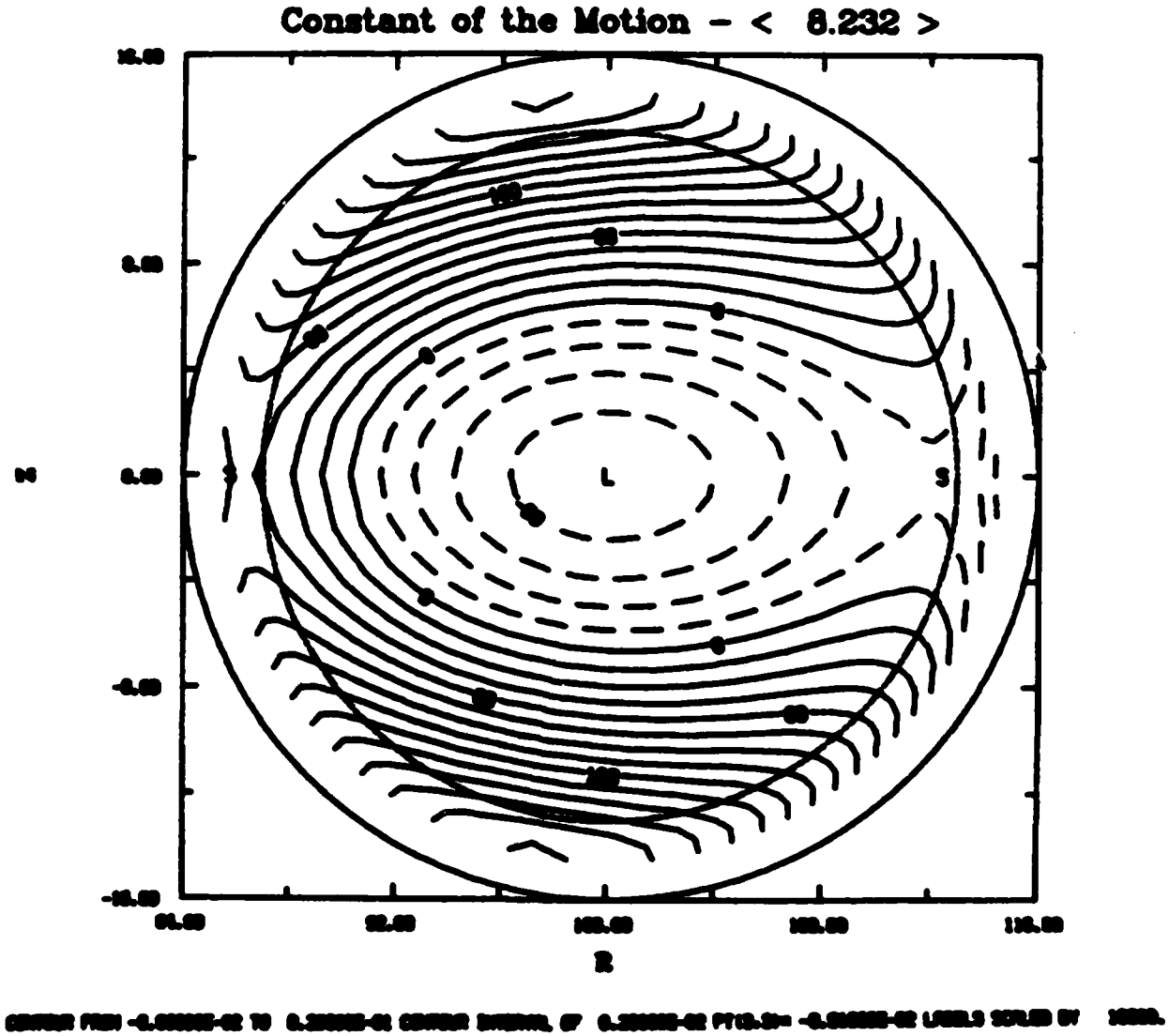

Fig. 8. Orbits of the ring centroid as in Fig. 6, but with n = 0.65.

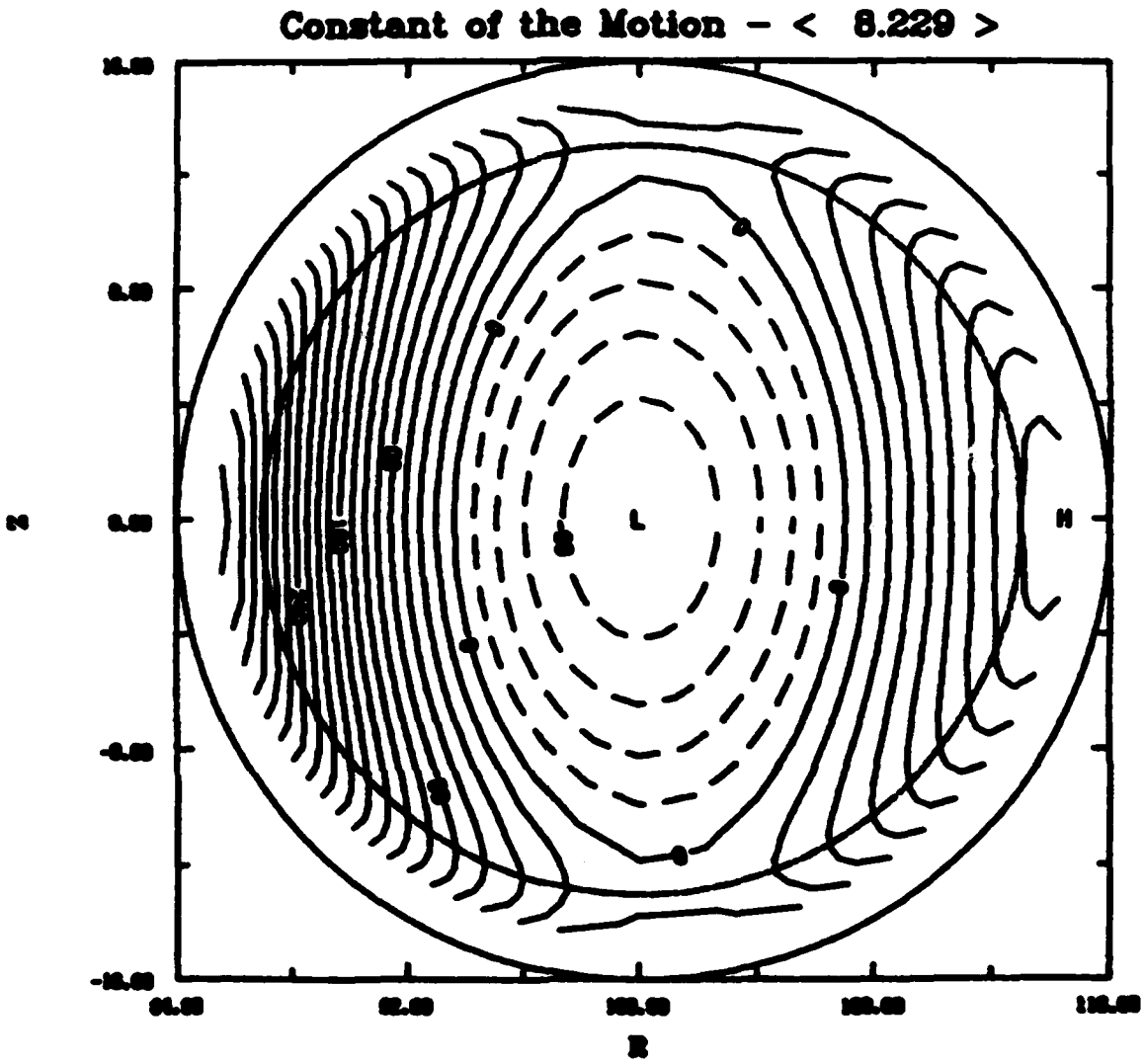

Fig. 9. Orbits of the ring centroid in the transverse plane from Eq. (7b) and the potentials of Eq. (10) for n = 0.35. The rest of the parameters as in Table II.

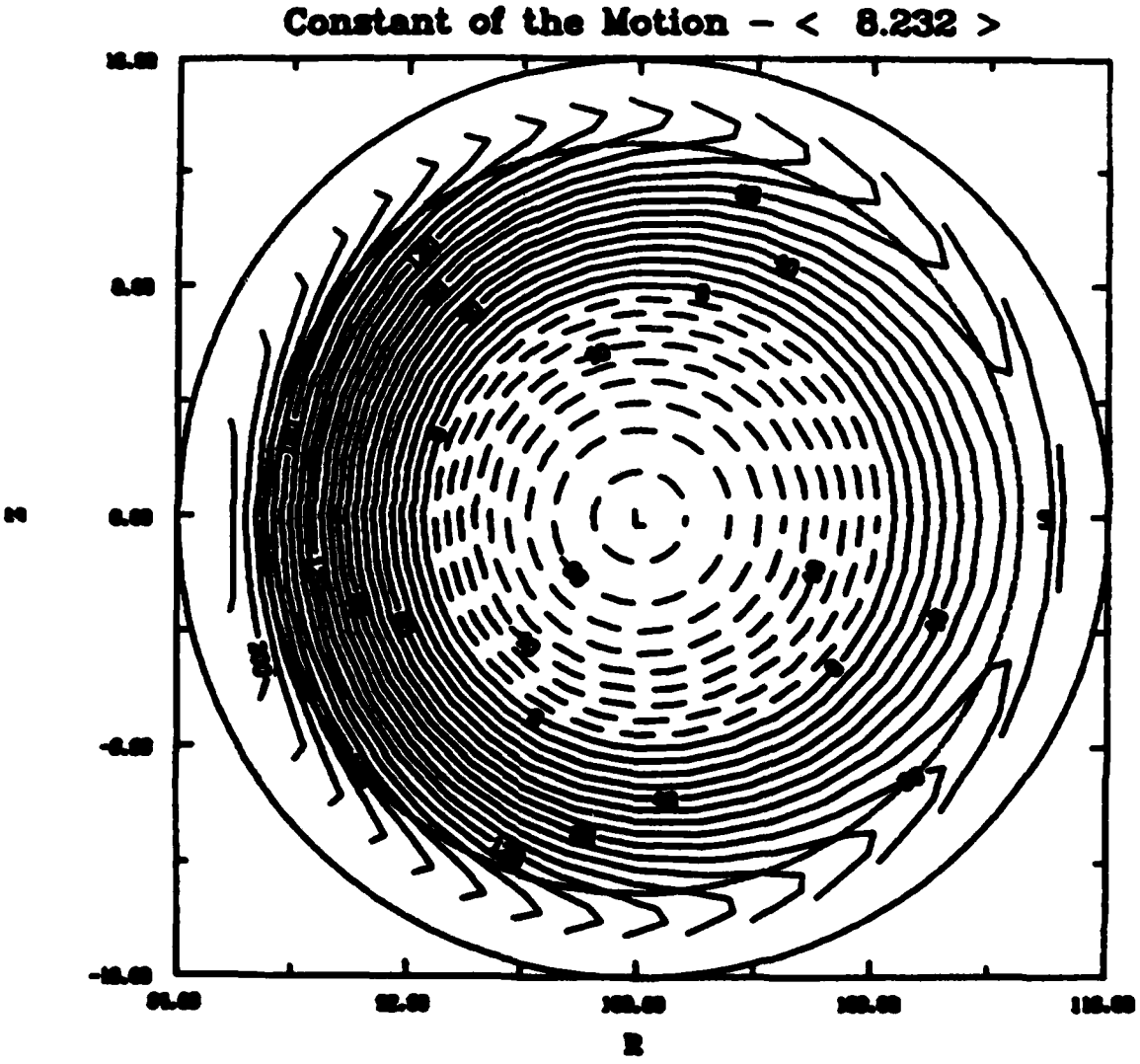

Fig.10. Orbits of the ring centroids in Fig. 9, but with n = 0.5.

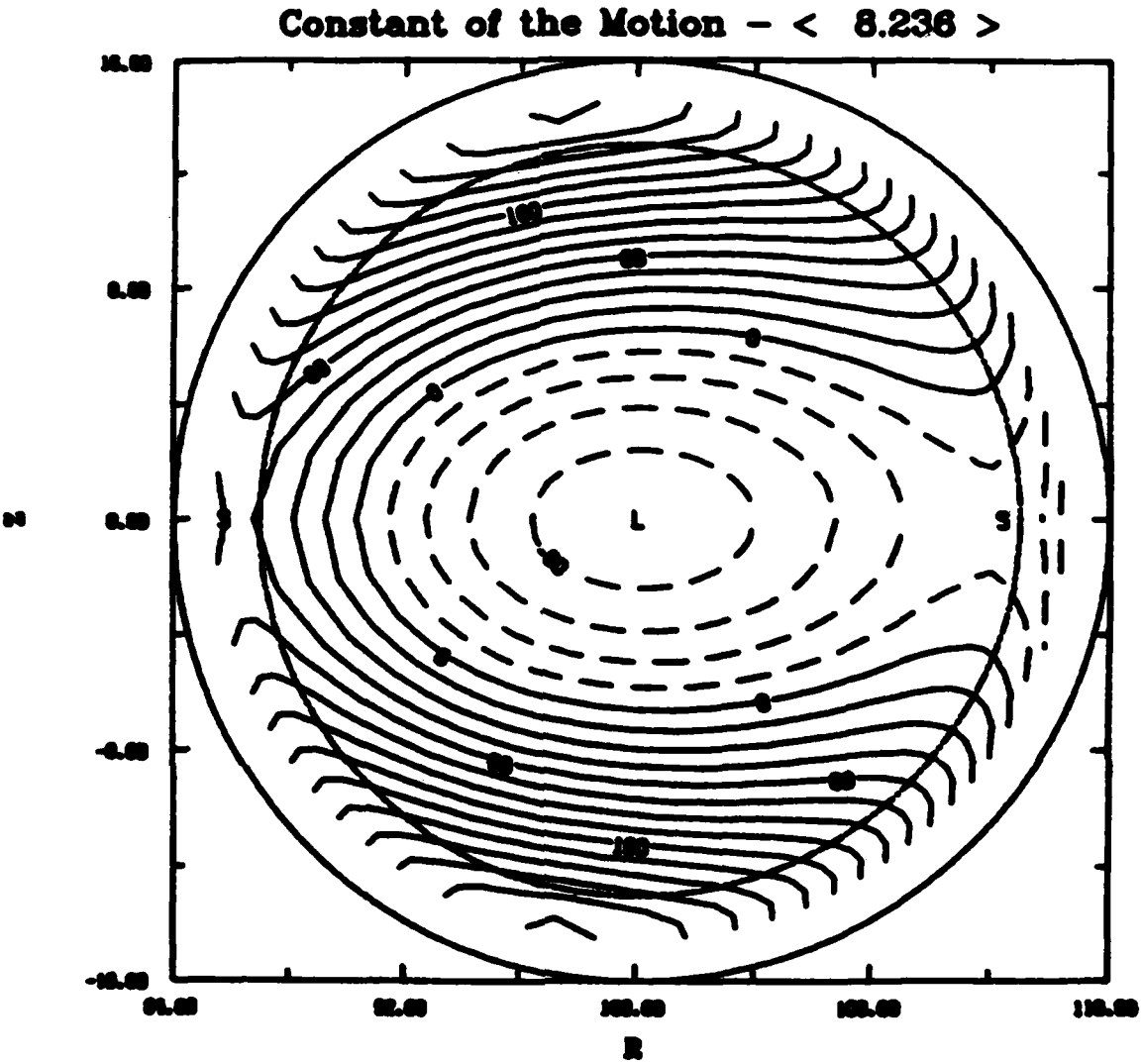

Fig.11. Orbits of the ring centroid as in Fig. 9, but with n = 0.65.

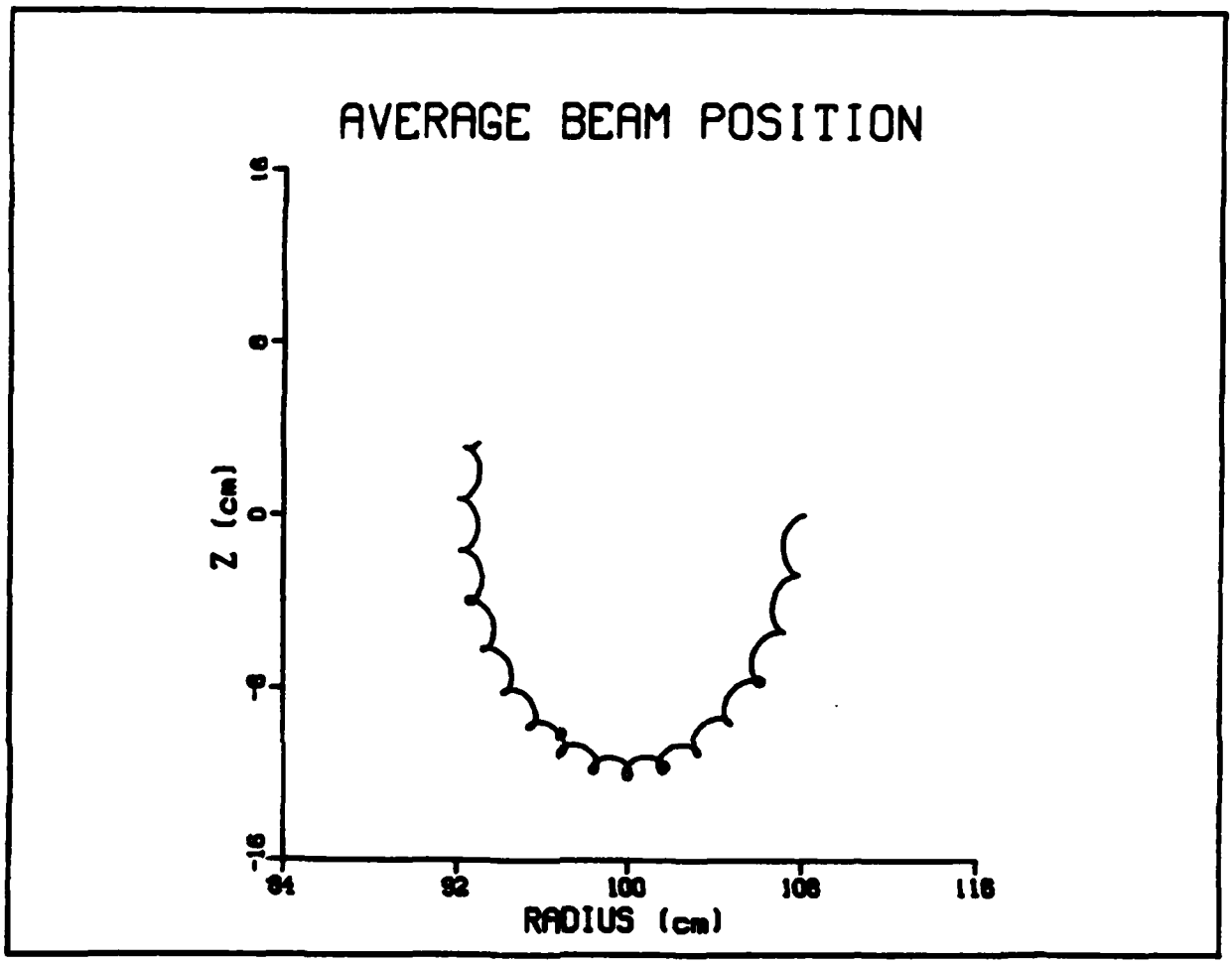

Fig.12. Computer simulation results showing the orbit of the ring centroid in the transverse plane for n = 0.35. The various parameters for this run are listed in Table III. The initial ring position was R = 108 cm, Z = 0.

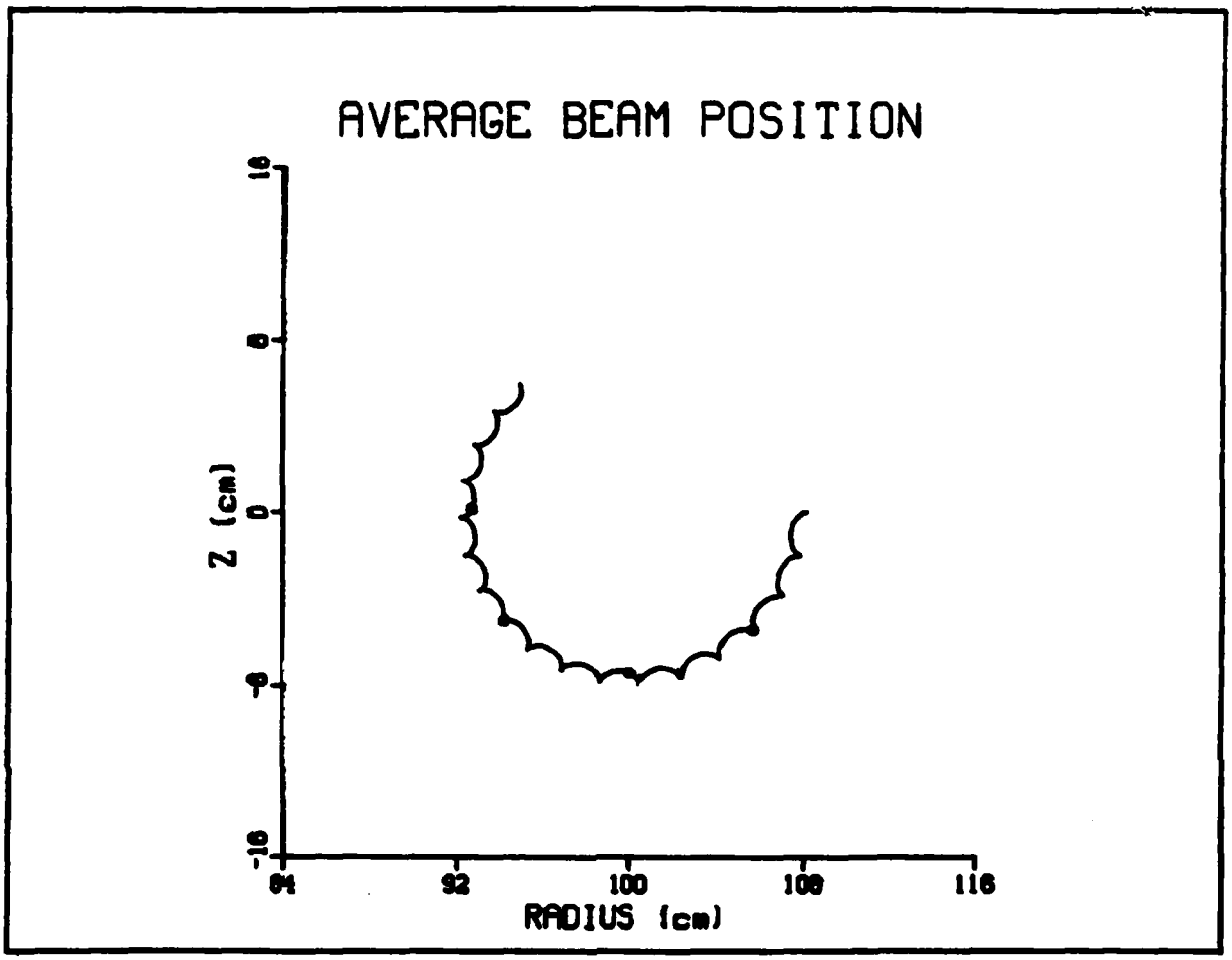

Fig.13. Computer simulation results showing the orbit of the ring centroid as in Fig. 12, but for n = 0.5.

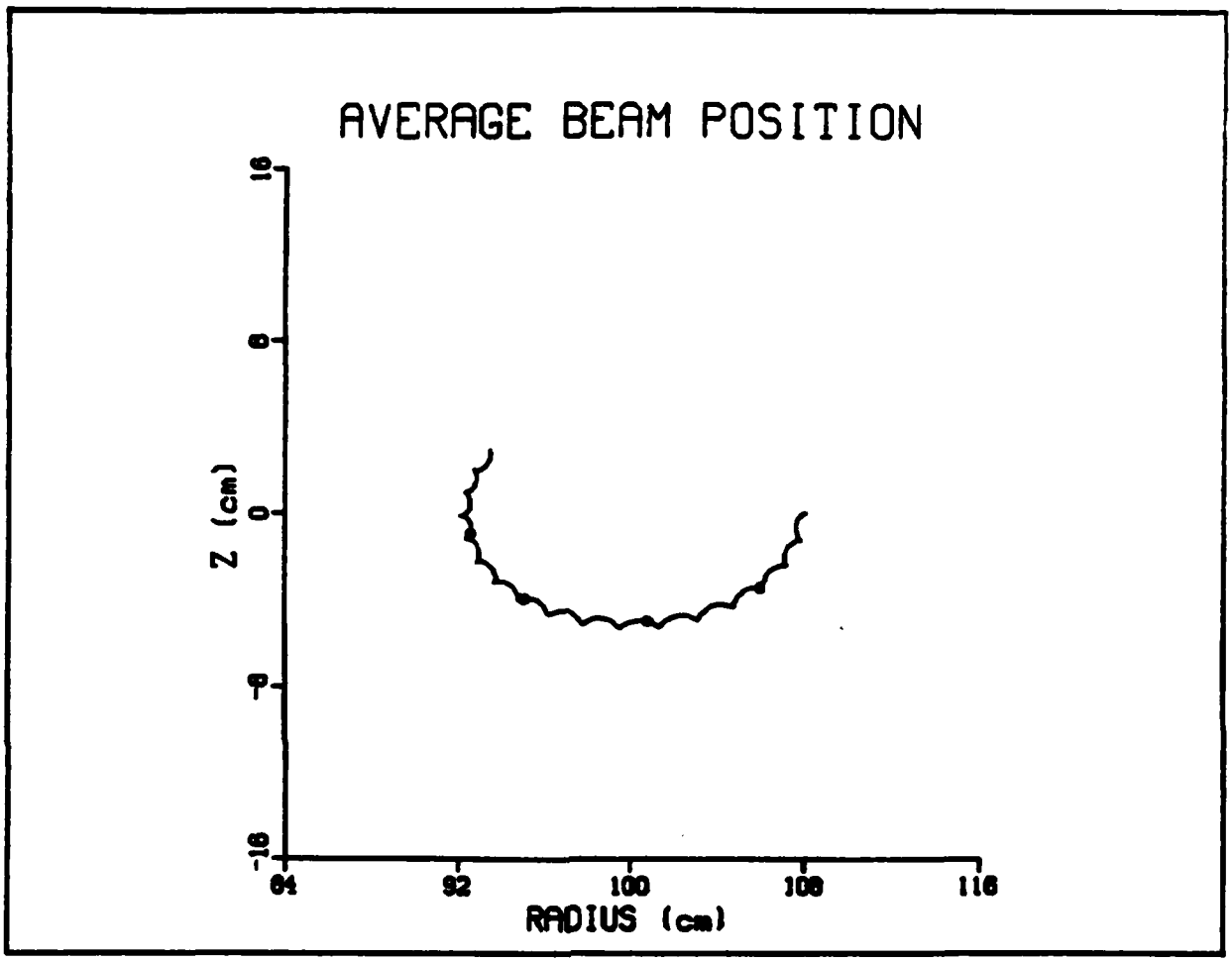

Fig.14. Computer simulation results showing the orbit of the ring centroid as in Fig. 12, but for n = 0.65.

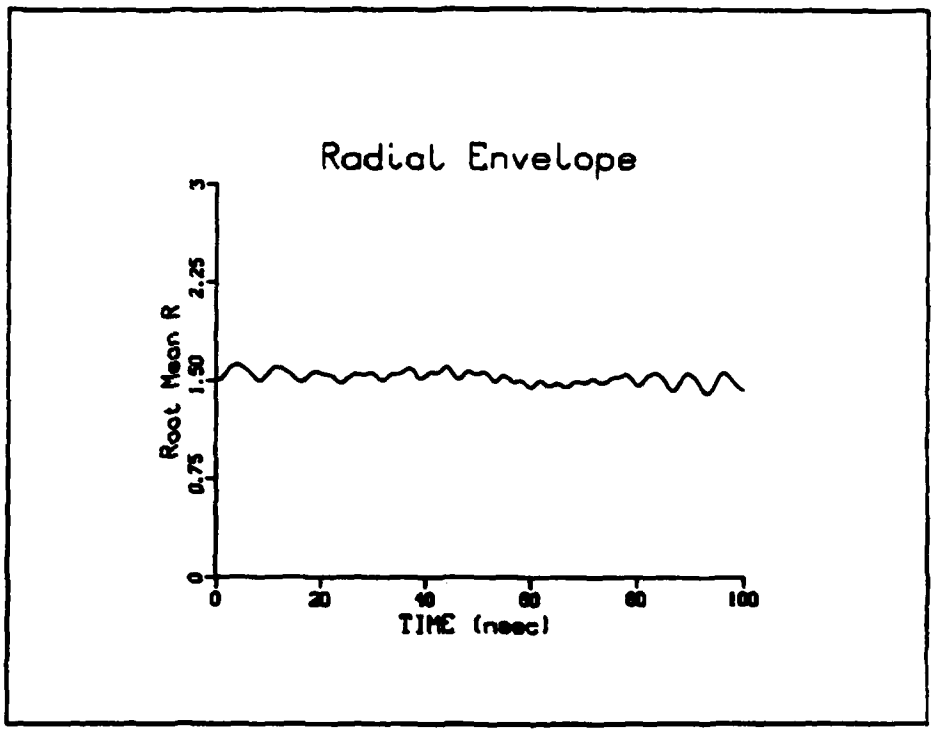

Fig.15a Radial ring envelope as a function of time for n = 0.5. The rest of the parameters as in Fig. 13.

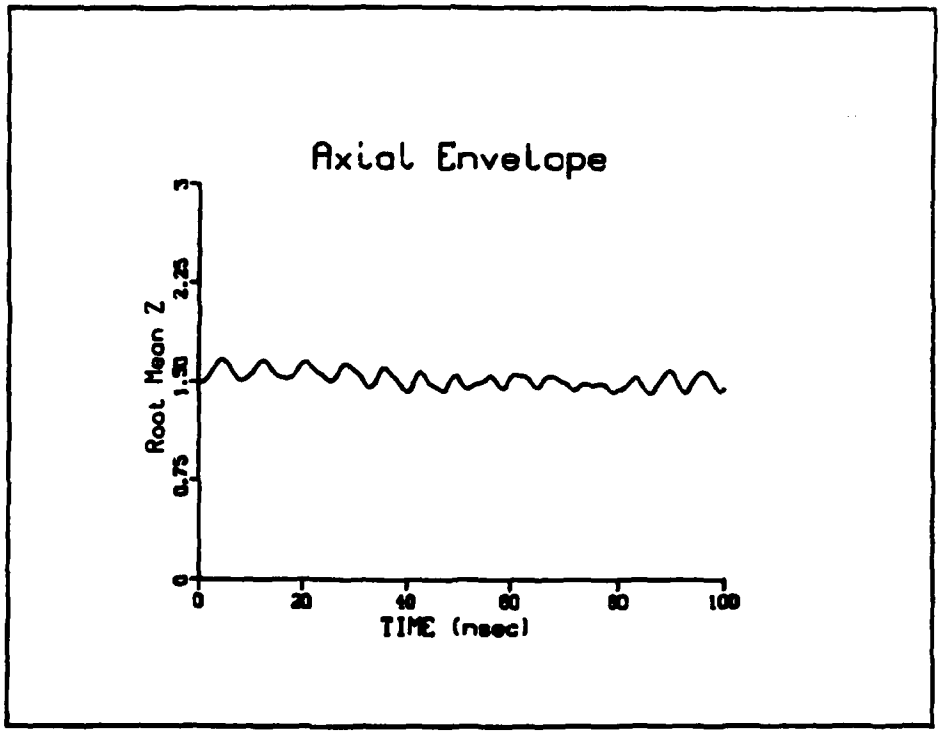

Fig.15b Axial ring envelope as a function of time for n = 0.5. The rest of the parameters as in Fig. 13.

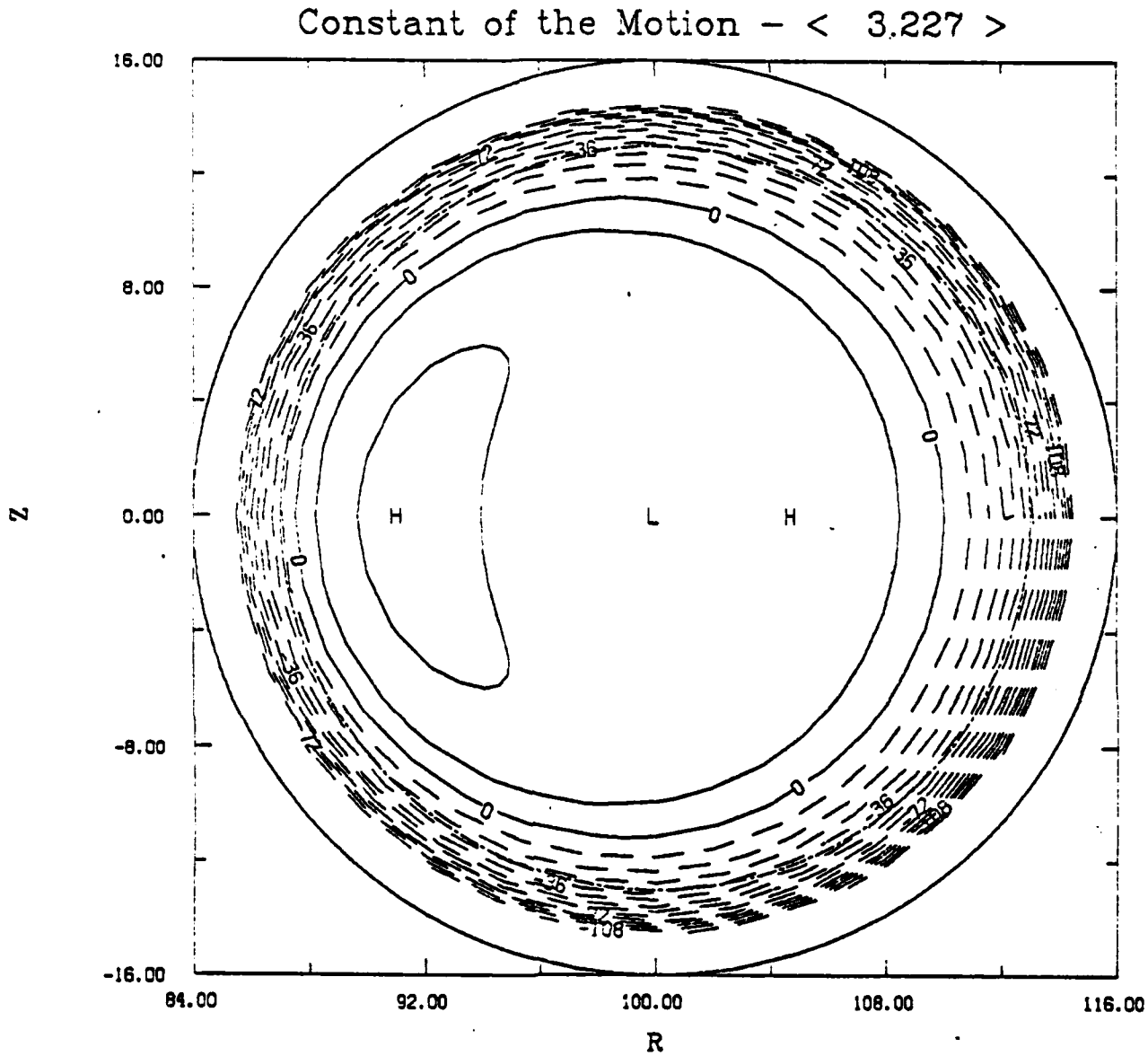

CONTOUR FROM -0.13500E-01 TO 0.18000E-02 CONTOUR INTERVAL OF 0.90000E-03 PT(3,3)= 0.13576E-02 LABELS SCALED BY 10000.

Fig.16. Orbits of the ring centroid in the transverse plane from Eq. (7b) and the potentials of Eq. (10) for $\gamma_o \approx 3$ and I = 1 KA. Th rest of the parameters are listed in Table IV.

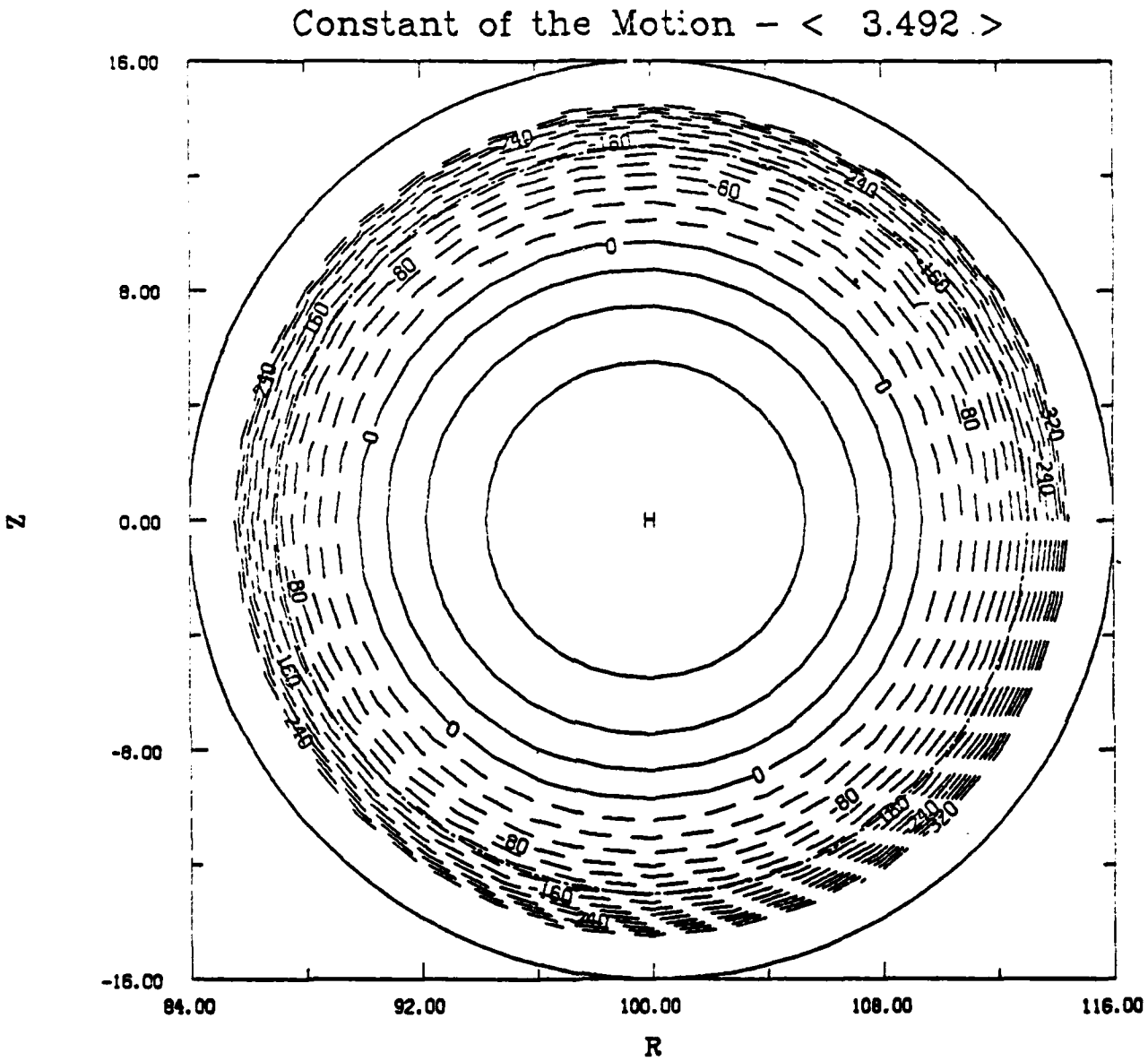

Fig.17. Orbits of the ring centroid as in Fig. 16, but with I = 2 KA.

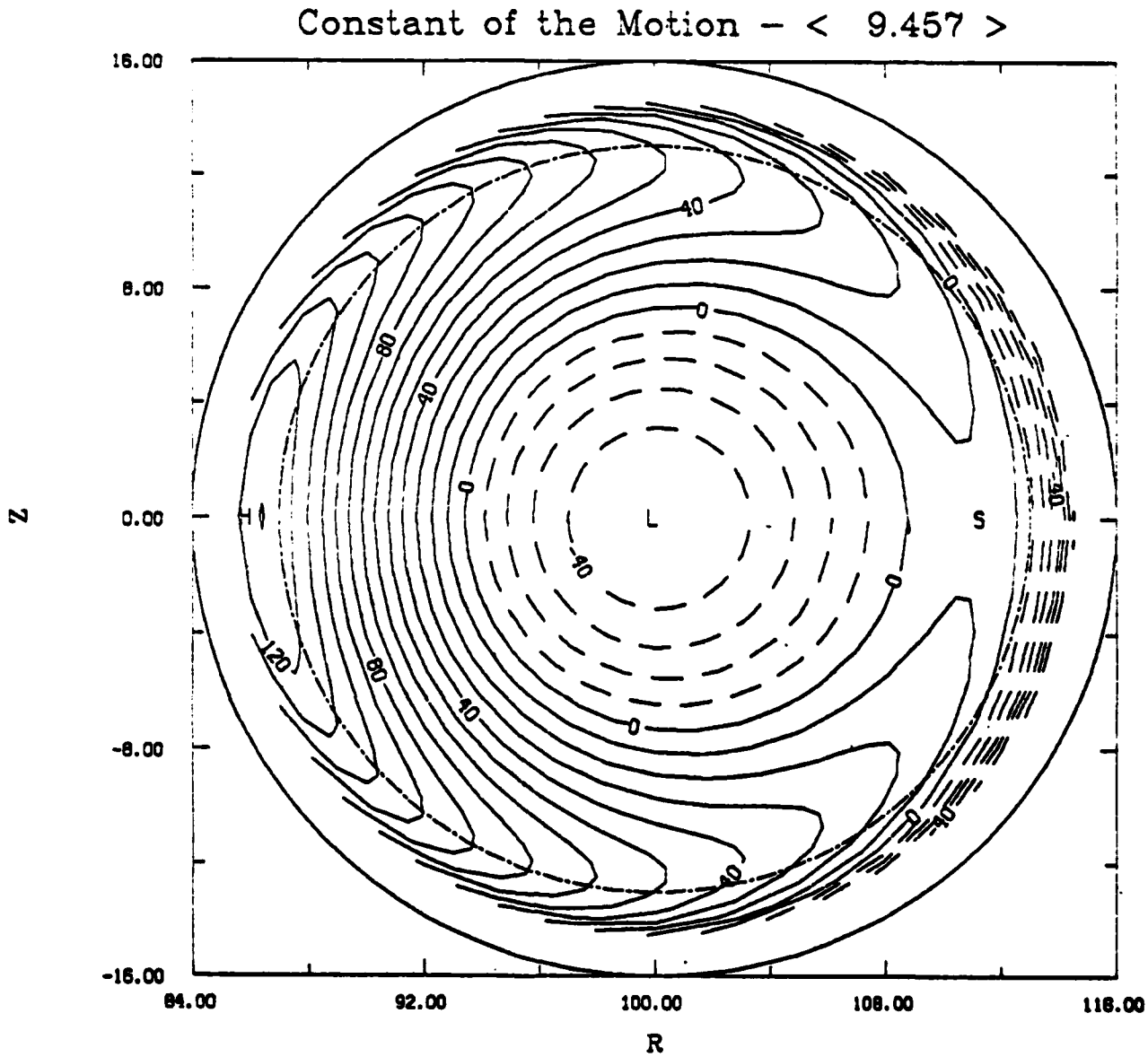

Fig.18. Orbits of the ring centroid as in Fig. 16, but with $\gamma = 7$ and $I = 10$ KA.

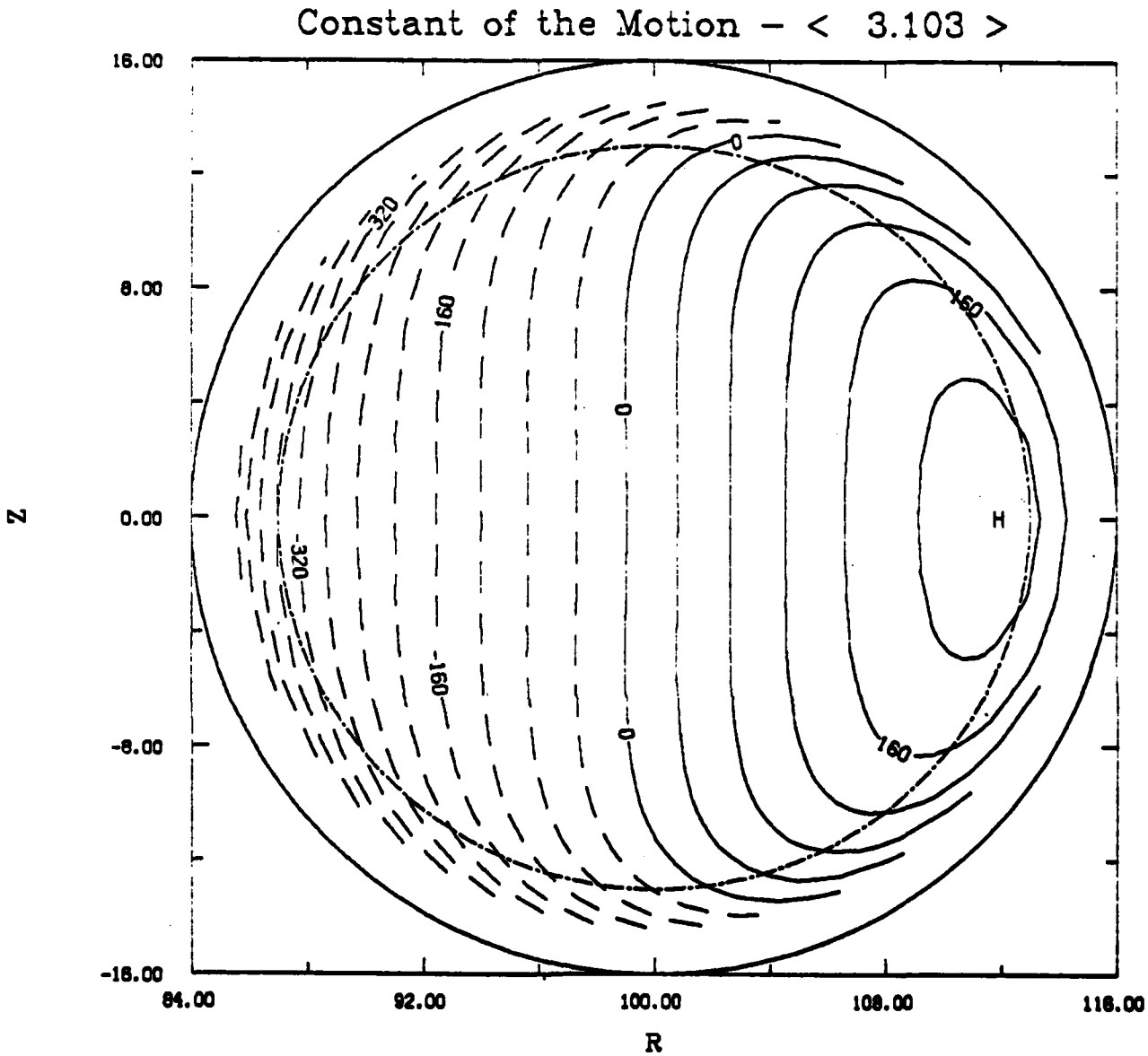

Fig.19. Orbits of the ring centroid as in Fig. 16, but with $\frac{P_\theta}{mcr_o} \neq 0$. The equilibrium position is shifted to the right.

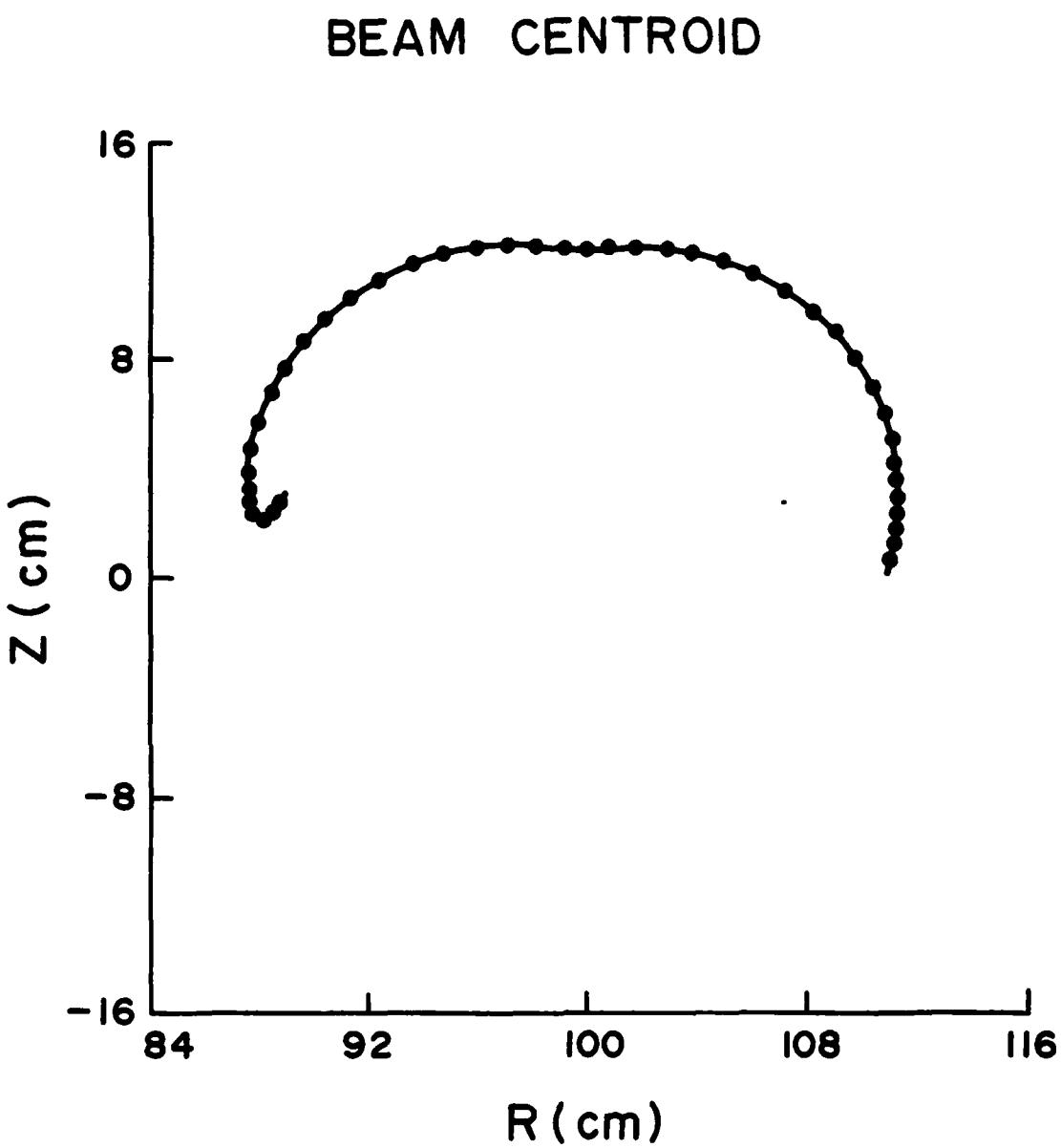

Fig.20a Computer simulation results showing the orbit of the ring centroid in the transverse plane. The time interval between two dots is 20 nsec. The various parameters for this run are listed in Table V. About 40 nsec before the end of the run the bounce frequency became zero without any noticeable disruption of the ring.

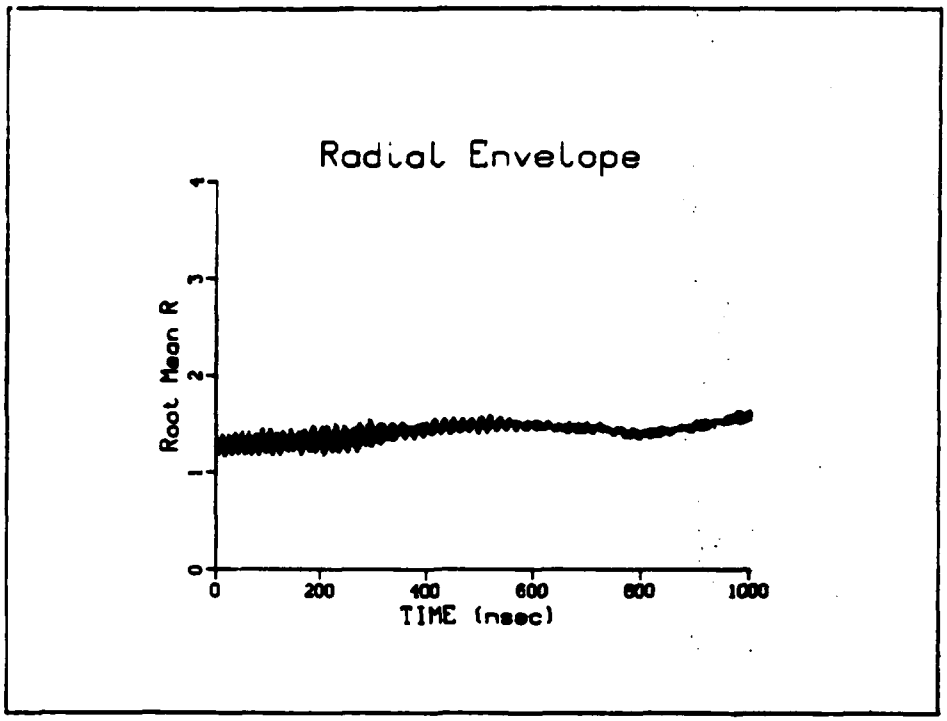

Fig.20b Radial ring envelope for the run of Fig. 20a.

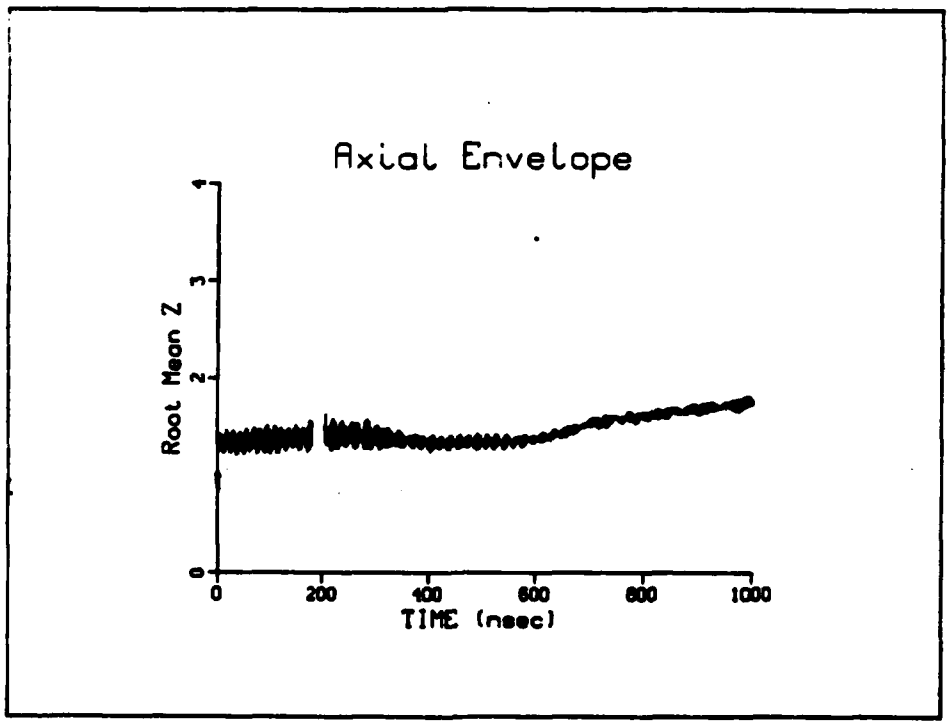

Fig.20c Axial ring envelope for the run of Fig. 20a.

Acknowledgments

We are grateful to several members of the Advanced Accelerator staff and in particular to Drs. P. Sprangle and Jeffry Golden for useful discussions and comments.

References

1. P. Sprangle and T. Coffey, Phys. Today, V. 37, No. 3, March 1984, p. 44.
2. Physics Today, B.G.L. [B. G. Levi], Vol. 36, No. 8, August 1983, p. 17.
3. C.A. Kapetanakos and P. Sprangle, NRL Memo Report #5259, 1984. AD-A142 302
4. N. Christofilos et al., Rev. Sci. Instrum. 35, 886 (1964).
5. J.E. Leiss, N.J. Norris and M. A. Wilson, Part. Acc. 10, 223 (1980).
6. D. Keefe, Part. Acc. 11, 187 (1981).
7. T.J. Fessenden, et al., High Power Beams 81, Proc. of the 4th Int. Topical Conf. on High-Power Electron and Ion-Beam Research and Technology, Palaiseau, France, June 29 - July 3, 1981, p. 813.
8. R. Briggs, Proc. 1981 Particle Accel. Conf., to be published in IEEE Trans. Nucl. Sci. NS-28 (June 1981).
9. A.I. Pavlovskii, et al., Sov. Phys. Dokl. 25, 120 (1980).
10. K.R. Prestwich, et al., IEEE Trans. on Nucl. Sci. NS-30, 3155 (1983).
11. L.N. Kazanskii, A.V. Kisletsov and A.N. Lebedev, Atomic Energy 30, 27 (1971).
12. M. Friedman, Appl. Phys. Lett. 41, 419 (1982).
13. D.W. Kerst, Nature 157, 90 (1946).
14. A.I. Pavlovskii, et al., Sov. Phys. Tech. Phys. 22, 218 (1977).
15. C.A. Kapetanakos, S.J. Marsh and P. Sprangle, NRL Memo Report # 5108 (1983); also Particle Accelerators 14, 261 (1984). AD-A133 291
16. A.G. Bonch-Osmolovskii, G.V. Dolbilow, I.N. Ivanov, E.A. Perelshtein, V.P. Sarantsev, O.I. Yarkovoy, JINR-Report P9-4135 Dubna (USSR) 1968.
17. P. Sprangle and C.A. Kapetanakos, J. Appl. Phys. 49, 1 (1978).
18. N. Rostoker, Comments on Plasma Physics, Cordon and Breach Science Publ. Inc., Vol. 6, p. 91 (1980).
19. P. Sprangle, C.A. Kapetanakos and S.J. Marsh, NRL Memo Report #4666 (1981). AD A108 359

20. C.A. Kapetanakos, P. Sprangle, D.P. Chernin, S.J. Marsh and I. Haber, NRL Memo Report # 4905 (1981); also Phys. of Fluids 26, 1634 (1983). AD-A119 869

21. C. W. Roberson, A. Mondelli and D. Chernin, Phys. Rev. Lett. 50, 507 (1983).

22. D. Chernin and P. Sprangle, Particle Accelerators 12, 85 (1982).

23. P. Sprangle and C.A. Kapetanakos, NRL Memo Report # 4950 (1983); also Particle Accelerators 14, 15 (1983). AD-A128 242

24. C.A. Kapetanakos, P. Sprangle and S.J. Marsh, Phys. Rev. Letts. 49, 741 (1982).

25. F. Mako et al., NRL Memo Report # 5196, 1983. AD-A134 694

26. C.A. Kapetanakos, P. Sprangle, NRL Memo Report #5259, 1984. AD-A142 302

EN

FILME

12-84

DTIC